12-2018

ADAPTIVE NONLINEAR MODEL REDUCTION FOR FAST POWER SYSTEM SIMULATION

Denis Osipov
University of Tennessee, dosipov@vols.utk.edu

To the Graduate Council:

I am submitting herewith a dissertation written by Denis Osipov entitled "ADAPTIVE NONLINEAR MODEL REDUCTION FOR FAST POWER SYSTEM SIMULATION." I have examined the final electronic copy of this dissertation for form and content and recommend that it be accepted in partial fulfillment of the requirements for the degree of Doctor of Philosophy, with a major in Electrical Engineering.

Kai Sun, Major Professor

We have read this dissertation and recommend its acceptance:

Leon M. Tolbert, Kevin L. Tomsovic, Xiaopeng Zhao

Accepted for the Council:
Carolyn R. Hodges

Vice Provost and Dean of the Graduate School

(Original signatures are on file with official student records.)

ADAPTIVE NONLINEAR MODEL REDUCTION

FOR FAST POWER SYSTEM SIMULATION

A Dissertation Presented for the

Doctor of Philosophy

Degree

The University of Tennessee, Knoxville

Denis Osipov

December 2018

DEDICATION

This dissertation is dedicated to my mother Vera Osipova.

ACKNOWLEDGEMENTS

I would like to thank my advisor Dr. Kai Sun for his guidance and always helpful advice during my doctoral studies and the research group colleagues Dr. Nan Duan, Dr. Fengkai Hu, Dr. Weihong Huang, Dr. Wenyun Ju, Dr. Chengxi Liu, Yang Liu, Dr. Junjian Qi, Hira Saleem, Dr. Bin Wang, Tianwei Xia, Xin Xu, Dr. Rui Yao, and Dr. Yongli Zhu for discussions and valuable suggestions.

I would like to thank my friends Anton Chertkovsky, Dr. Cheryl Dalid, Dr. Yasser Ashraf Gandomi, Christos Giannopoulos, Dr. Valeria Stefania Lopes Caitar, Dr. Artem Maksov, Dr. Manuela Picariello and Dr. Aditi Rambani for their support during my time as a PhD student.

I would also like to thank Dr. Srdjan Simunovic, Dr. Srikanth Allu, and Dr. Aleksandar Dimitrovski for the interesting and productive collaboration on a project with the Oak Ridge National Laboratory.

Finally, I am very thankful to members of my dissertation committee Dr. Leon M. Tolbert, Dr. Kevin L. Tomsovic and Dr. Xiaopeng Zhao for their time and effort.

This work was supported in part by UT-Battelle, LLC under Contract No. DE-AC0500OR22725 with the U.S. Department of Energy, in part by the National Science Foundation under Grant No. ECCS-1610025, and in part by the Engineering Research Center Program of the National Science Foundation and the Department of Energy under Grant No. EEC-1041877.

ABSTRACT

The dissertation proposes a new adaptive approach to power system model reduction for fast and accurate time-domain simulation. This new approach is a compromise between linear model reduction for faster simulation and nonlinear model reduction for better accuracy. During the simulation period, the approach adaptively switches among detailed and linearly or nonlinearly reduced models based on variations of the system state: it employs unreduced models for the fault-on period, uses weighted column norms of the admittance matrix to decide which functions are to be linearized in power system differential-algebraic equations for large changes of the state, and adopts a linearly reduced model for small changes of the state.

Two versions of the adaptive model reduction approach are introduced. The first version uses traditional power system partitioning where the model reduction is applied to a defined large external area in a power system and the other area that is defined as the study area keeps full detailed models. The second version applies the adaptive model reduction to the whole system.

Speed improvement techniques using parallelization are investigated. The first technique uses parallelism in space; it further divides the study area into subareas that can be simulated in parallel. The second technique uses parallelism in time; it integrates the adaptive model reduction into the coarse solver of the Parareal method.

In addition, the dissertation proposes integration of tensor decomposition into the adaptive model reduction approach to further improve the speed and accuracy of simulation.

All proposed approaches are validated by comprehensive case studies on the 140-bus 48-machine Northeast Power Coordinating Council system, 2383-bus 327-machine Polish system, and 5617-machine 70285-bus Eastern Interconnection system using different dynamic models.

TABLE OF CONTENTS

LIST OF TABLES

LIST OF FIGURES

CHAPTER ONE

INTRODUCTION AND BACKGROUND INFORMATION

1.1 Introduction

Power system simulation is very important for grid operations and planning at electricity utilities. It can assess dynamic security under a certain operating condition of the studied power system following a given contingency such as loss of a transmission line or generator unit. Essentially, power system simulation is to obtain a time-series trajectory of the system state for a specified simulation window by solving the initial value problem of a set of nonlinear differential-algebraic equations co-determined by the mathematical model of the whole system, the operating condition and the contingency. Nowadays, the fast growth in electricity demand and a relatively slow construction of new transmission infrastructure are pushing power transmission systems to be operated closer to their stability limits and motivating the transition of power system simulation from the offline planning stage to the real-time operation environment.

1.2 Model Reduction

One way to increase the speed of simulation of a complex power grid is to conduct network partitioning and then model reduction. For example, a traditional approach defines a study area, which is an important small part of the system for dynamic security assessment, considering all the details, and reduces the model of the rest of the system, i.e.

the external area. In practice, an additional buffer zone is often defined in between with moderate reduction to connect the study and the external areas [1]. The methods for model reduction on the external area can be divided into two main groups: the ones that preserve the structure of a power system and the ones that use mathematical transformations from original states to nonphysical states that are subsequently reduced.

1.2.1 Coherency based model reduction methods

The most widely used methods from the first group are coherency-based methods [2]-[11], which were originally developed for power system model reduction and conduct the following steps: coherency identification, aggregation of coherent generators, and network reduction. After the first step, the generators that oscillate together following a disturbance are included into one group. The groups of coherent generators are then aggregated into individual equivalent generators connected with each other by equivalent branches and with the study area by a reduced system network. This creates a unique boundary between the external area and the study area and does not allow arbitrary division between areas. In addition, if the topology of the original system changes, it can affect the coherency and consequently the split between the study area and the generator grouping of the external area. This can change the boundary in between. Thus, the grouping of generators based on coherency has an inherent limitation on the way a system can be partitioned.

1.2.2 Model reduction methods from automatic control field

The second group of methods does not have that limitation as the states are transformed into a new state space. Thus, the system can be partitioned in any way. These methods came from the control field of engineering. In the most used methods from this category, the external area model is first linearized and then reduced using balanced truncation [12]-[16] or Krylov subspace methods [17]-[20]. The linearization of the model gives acceptably accurate results when concerned disturbances are small but once the size of the disturbance increases the linearized model cannot guarantee an accurate representation of the original part of the system. To improve the accuracy of large-disturbance simulation, nonlinear model reduction methods can be used. References [21]-[22] propose using empirical controllability and observability covariance matrices that contain nonlinear behavior of the system around the operating condition. In [23]-[24] the authors try to generalize and extend the linear balance truncation to nonlinear systems. A proper orthogonal decomposition method is described in [25], whose error and computational complexity are analyzed. As shown in [25]-[26], application of nonlinear model reduction cannot substantially decrease computational time as compared to the original model. In addition, some methods require training simulation data to create a reduced model, which cannot guarantee adequate performance during all possible disturbances. If a disturbance is very different from that with the training set, the model reduction error can substantially increase [27].

1.3 Parareal Method

In the existing literature, three directions of computational acceleration by parallelism for power system simulation have been explored. They are spatial [28]-[29], temporal [30]-[32] and across solution methods [33]-[34]. Parareal is a parallel computing algorithm based on the decomposition of the temporal domain into separate (coarse) subintervals. The algorithm is based on prediction-correction iterations between a sequential (coarse, approximate, fast), and concurrent (fine, accurate) integrators. The overall speedup is controlled by the performance of the coarse solver and, in the ideal case, it scales as the ratio of the number of coarse intervals over the number of iterations. However, for nonlinear power system problems, the time spent on propagating the coarse solution is not negligible [32], and it may take a large portion of the total consumed time. To improve the coarse solver performance, [31] used lower order generator model for the coarse solver, but the improvement was marginal.

1.4 Tensor Decomposition

Application of tensor decomposition in model reduction is a relatively new and growing scope of research [35-37]. The idea of the approach is to convert a large matrix into a tensor (represented by a multidimensional array) and apply tensor decomposition to represent this tensor as a set of small matrices, which can be converted back to the original matrix formulation with a sufficiently small error. Operations with these small matrices require less memory and computing power compared to the original large matrix and can increase the computational speed. In dynamic system simulation, the tensor decomposition

can be used to reduce the calculation time of higher terms of Taylor series expansion [38-39].

1.5 Contribution of this Work

Compared to the existing work, this dissertation proposes a new adaptive model reduction approach, which is a compromise between linear model reduction and nonlinear model reduction in terms of accuracy and speed of time-domain simulation using the reduced model. A comprehensive study is also presented to compare this adaptive model reduction approach with the linear model reduction approach and the coherency-based model reduction approach. During the simulation period, the approach adaptively switches among detailed and linearly or nonlinearly reduced models based on variations of the system state: it employs unreduced models for the fault-on period, uses weighted column norms of the admittance matrix to decide which functions need to be linearized in the power system model for large changes of the state, and adopts a linearly reduced model for small changes of the state.

The version of the adaptive approach described above uses traditional topological power system partitioning with the study area and the external area. This partitioning creates an additional error that can affect the performance of the model reduction. To address the partitioning error, the second version of the adaptive approach is proposed where the model reduction is performed to the whole system.

The main contributions of this work are in the following aspects:

- a new model reduction approach is proposed that enables adaptive switching among the detailed model, the linear reduced model and the hybrid reduced model having only certain functions linearized;
- unlike most of existing model reduction methods that need to partition the whole power network into a study area with detailed models and external area with reduced models, the new approach can be applied to either a partitioned external area only or the whole system without network partitioning;
- application of power system model reduction of the system with multiple study areas that can be simulated in parallel;
- application of adaptive model reduction as the coarse solver of the Parareal method;
- integration of tensor decomposition to the adaptive model reduction.

CHAPTER TWO

ADAPTIVE NONLINEAR MODEL REDUCTION

2.1 Power System Partitioning

As it was mentioned in chapter one, in power system model reduction the system is divided into two areas: 1) the study area, which is the main interest of an investigator, where all details are preserved, and all disturbances are originated from; 2) the external area, which can be simplified and reduced. The partitioned power system is shown in Figure 2.1.

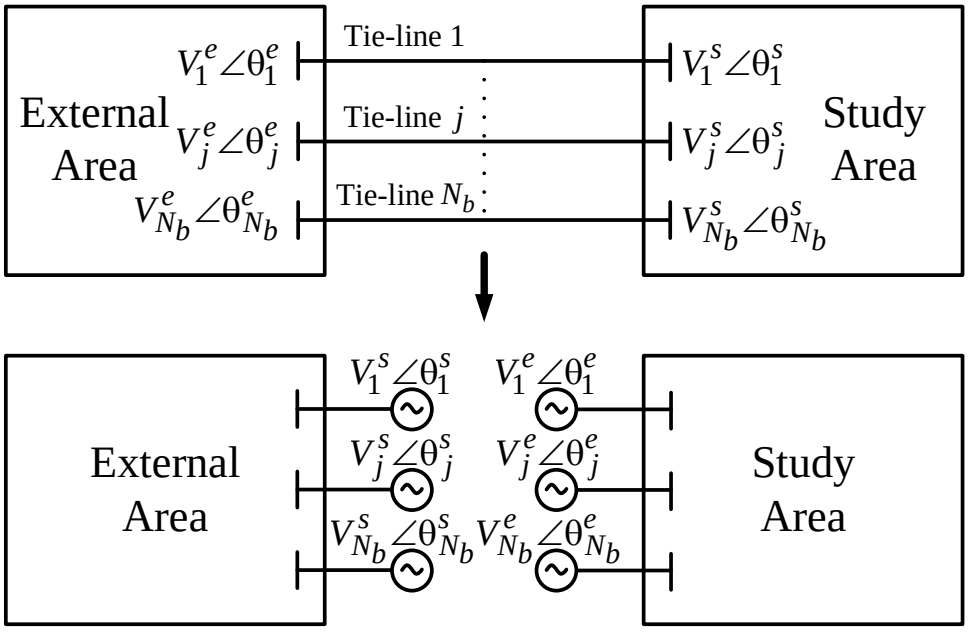

Figure 2.1. Power system partitioning.

The study area of the original system is connected to the external area by several tie-lines. For the study area, a tie-line *j* is treated as a simple fictitious generator with the internal voltage phasor equal to a voltage phasor $V_j^e \angle \theta_j^e$ of the corresponding boundary bus in the external area and with the armature resistance and transient reactance equal to the resistance and reactance of a tie-line *j*. Likewise for the external area, a tie-line *j* is treated as a generator with the internal voltage phasor equal to a voltage phasor $V_j^s \angle \theta_j^s$ of the corresponding boundary bus in the study area. During each iteration of the system simulation these fictitious generators are treated as constant voltage sources and represent the current injections from one area to the other area. Therefore, voltage magnitudes and voltage angles of boundary buses in one area are the inputs to the model of the other area. At every iteration, each area is calculated separately, then the boundary bus voltage phasors of both areas are recalculated, and their values are sent as inputs to the corresponding area to perform the next iteration. As constant voltage sources the fictitious generators do not have inertias or contribute to the dynamics of each area as a component of the differential equations of generators inside the corresponding area.

In this chapter, each generator is represented by a detailed two-axis model with a non-reheat steam turbine model, a first-order governor model and an IEEE type 1 exciter model [40], as described be these nine differential equations:

$$
\begin{cases}
\dot{\delta}_i = \omega_{base}\left(\omega_i - 1\right) \\
T_{ch_i}\dot{P}_{m_i} = -P_{m_i} + P_{gv_i} \\
T_{gv_i}\dot{P}_{gv_i} = -P_{gv_i} + P_{ref_i} - \dfrac{\left(\omega_i - 1\right)}{R_i} \\
T_{A_i}\dot{V}_{R_i} = -V_{R_i} + K_{A_i}R_{f_i} - \dfrac{K_{A_i}K_{F_i}}{T_{F_i}}E_{fd_i} + K_{A_i}\left(V_{ref_i} - V_{t_i}\right) \\
T_{F_i}\dot{R}_{f_i} = -R_{f_i} + \dfrac{K_{F_i}}{T_{F_i}}E_{fd_i} \\
T_{E_i}\dot{E}_{fd_i} = -\left(K_{E_i} + A_{E_i}e^{B_{E_i}E_{fd_i}}\right)E_{fd_i} + V_{R_i} \\
T'_{qo_i}\dot{E}'_{d_i} = -E'_{d_i} + \left(X_{q_i} - X'_{q_i}\right)I_{q_i} \\
T'_{do_i}\dot{E}'_{q_i} = -E'_{q_i} - \left(X_{d_i} - X'_{d_i}\right)I_{d_i} + E_{fd_i} \\
2H_i\dot{\omega}_i = P_{m_i} - E'_{d_i}I_{d_i} - E'_{q_i}I_{q_i} - D_i\left(\omega_i - 1\right)
\end{cases}
\tag{2.1}
$$

where

$$
I_{d_i} = \sum_{j=1}^{N_g} E'_{d_j}\left[G_{ij}\cos(\delta_i - \delta_j) + B_{ij}\sin(\delta_i - \delta_j)\right] + \sum_{j=1}^{N_g} E'_{q_j}\left[G_{ij}\sin(\delta_i - \delta_j) - B_{ij}\cos(\delta_i - \delta_j)\right]
$$

$$
+ \sum_{j=1}^{N_b} V_j\left[G_{ij}\sin(\delta_i - \theta_j) - B_{ij}\cos(\delta_i - \theta_j)\right],
$$

$$
I_{q_i} = \sum_{j=1}^{N_g} E'_{d_j}\left[-G_{ij}\sin(\delta_i - \delta_j) + B_{ij}\cos(\delta_i - \delta_j)\right] + \sum_{j=1}^{N_g} E'_{q_j}\left[G_{ij}\cos(\delta_i - \delta_j) + B_{ij}\sin(\delta_i - \delta_j)\right]
$$

$$
+ \sum_{j=1}^{N_b} V_j\left[G_{ij}\cos(\delta_i - \theta_j) + B_{ij}\sin(\delta_i - \theta_j)\right],
$$

Here, δ_i and ω_i are the rotor angle and speed of generator *i* in rad and p.u., respectively; $\omega_{base} = 120\pi$ rad/s is the base speed; P_m, P_{gv_i} and P_{ref_i} are the mechanical power,

governor output power and reference power all in p.u.; R_i is the speed regulation factor; E'_{d_i}, E'_{q_i}, X_{d_i}, X_{q_i}, X'_{d_i}, X'_{q_i}, I_{d_i} and I_{q_i} are respectively the d- and q-axis internal voltages, synchronous reactances, transient reactances and currents all in p.u.; V_{R_i}, K_{A_i}, R_{f_i}, K_{F_i}, E_{fd_i}, V_{ref_i}, V_{t_i}, K_{E_i}, A_{E_i} and B_{E_i} are the voltage regulator input, amplifier gain, rate feedback, feedback gain, field voltage, reference voltage, terminal bus voltage, exciter gain and exciter saturation coefficients all in p.u.; time constants H_i, T_{ch_i}, T_{gv_i}, T_{A_i}, T_{F_i}, T_{E_i}, T'_{qo_i} and T'_{do_i} are respectively the generator inertia, turbine charging time, governor time constant, amplifier time constant, feedback time constant, exciter time constant, q-axis open circuit time constant and d-axis open circuit time constant all in s; D_i, is the damping coefficient in p.u.; N_g is the number of generators; N_b is the number of boundary buses; G_{ij} and B_{ij} are conductance and susceptance between generator *i* and generator *j*. in p.u.; V_j is the voltage magnitude at boundary bus *j* in the opposite area in p.u.; θ_j is the voltage angle at boundary bus j in the opposite area in rad.

2.2 Model Reduction

If model reduction is applied to the external area, it is necessary to define state variables and inputs of the system. Considering that every generator is described by nine differential equations and every boundary bus has the voltage magnitude and angle as its parameters, let $n = 9N_g$ and $m = 2N_b$ respectively denote the numbers of state variables

and inputs of the external area, and let the outputs of the system be the state variables of the system.

Then the system (2.1) can be described as the nonlinear system:

$$\begin{cases} \dot{\mathbf{x}} = \mathbf{f}\left(\mathbf{x}, \mathbf{u}\right) \\ \mathbf{y} = \mathbf{x} \end{cases} \tag{2.2}$$

where

$$\mathbf{x} = \begin{pmatrix} \boldsymbol{\delta} & \mathbf{P}_m & \mathbf{P}_{gv} & \mathbf{V}_R & \mathbf{R}_f & \mathbf{E}_{fd} & \mathbf{E}'_d & \mathbf{E}'_q & \boldsymbol{\omega} \end{pmatrix}^T, \qquad \mathbf{u} = \begin{pmatrix} \boldsymbol{\theta} & \mathbf{V} \end{pmatrix}^T,$$

$\mathbf{x} \in \mathrm{R}^n$ is the state vector; $\mathbf{u} \in \mathrm{R}^m$ is the input vector; $\mathbf{y} \in \mathrm{R}^n$ is the output vector.

2.2.1 Linear model reduction

The system (2.2) can be linearized around an equilibrium point as:

$$\begin{cases} \Delta\dot{\mathbf{x}} = \mathbf{A}\Delta\mathbf{x} + \mathbf{B}\Delta\mathbf{u} \\ \Delta\mathbf{y} = \mathbf{C}\Delta\mathbf{x} \end{cases} \tag{2.3}$$

where $\Delta\mathbf{x}$, $\Delta\mathbf{u}$ and $\Delta\mathbf{y}$ are the deviation variables of respectively the original states, inputs and outputs; $\mathbf{A} \in \mathrm{R}^{n\times n}$ is the matrix of partial derivatives of the functions in (2.1) with respect to each state variable evaluated at the equilibrium point; $\mathbf{B} \in \mathrm{R}^{n\times m}$ is the matrix of partial derivatives of the functions in (2.1) with respect to each input variable evaluated at the equilibrium point; $\mathbf{C} \in \mathrm{R}^{n\times n}$ is the identity matrix.

The system (2.3) can be reduced using a linear reduction method, for example, the balanced truncation method [12]. To apply this method Lyapunov equations are solved to obtain controllability Gramian $\mathbf{W}_c$ and observability Gramian $\mathbf{W}_o$:

$$\begin{cases} \mathbf{A}\mathbf{W}_c + \mathbf{W}_c\mathbf{A}^T + \mathbf{B}\mathbf{B}^T = \mathbf{0} \\ \mathbf{A}^T\mathbf{W}_o + \mathbf{W}_o\mathbf{A} + \mathbf{C}^T\mathbf{C} = \mathbf{0} \end{cases} \tag{2.4}$$

The Gramians are then used to calculate transformation matrix $\mathbf{T}$ and its inverse $\tilde{\mathbf{T}}$.

Matrix $\mathbf{T}$ transforms the states from the original state space to a new balanced state space: $\Delta\tilde{\mathbf{x}} = \mathbf{T}\Delta\mathbf{x}$.

In the resulting new balanced system, the states are arranged in a such way that the first state is the most controllable and the most observable and the last state is the least controllable and the least observable. Henkel singular values show this relationship:

$$\sigma_1 > \sigma_2 > \cdots > \sigma_i > \cdots > \sigma_{n-1} > \sigma_n \geq 0, \tag{2.5}$$

where

$$\sigma_i = \sqrt{\lambda_i\left(\mathbf{W}_c\mathbf{W}_o\right)} = \Sigma_{ii}.$$

Considering the above-mentioned fact, only the first r states can be kept and the rest can be truncated. H_∞ norm of the error of balanced truncation is bounded by the following expression:

$$\left\|\varepsilon\right\|_\infty \leq 2\sum_{i=r+1}^{n}\sigma_i. \tag{2.6}$$

The transformation matrix and its inverse are recalculated as follows:

$$\mathbf{T} = \mathbf{P}\mathbf{T}, \qquad \tilde{\mathbf{T}} = \tilde{\mathbf{T}}\mathbf{P}^T, \tag{2.7}$$

where $\mathbf{P} = \begin{pmatrix}\mathbf{I} & \mathbf{0}\end{pmatrix}$ is the identity matrix, the last $(n-r)$ rows of which are deleted.

Thus, the balanced truncated system is represented as follows:

$$\begin{cases} \Delta\dot{\tilde{\mathbf{x}}} = \mathbf{T}\mathbf{A}\tilde{\mathbf{T}}\Delta\tilde{\mathbf{x}} + \mathbf{T}\mathbf{B}\Delta\mathbf{u} \\ \Delta\mathbf{y} = \mathbf{C}\tilde{\mathbf{T}}\Delta\tilde{\mathbf{x}} \end{cases} \tag{2.8}$$

The system in (2.8) can be written in a more compact form:

$$\begin{cases} \Delta\dot{\tilde{\mathbf{x}}} = \tilde{\mathbf{A}}\Delta\tilde{\mathbf{x}} + \tilde{\mathbf{B}}\Delta\mathbf{u} \\ \Delta\mathbf{y} = \tilde{\mathbf{C}}\Delta\tilde{\mathbf{x}} \end{cases} \tag{2.9}$$

where

$$\tilde{\mathbf{A}} = \mathbf{T}\mathbf{A}\tilde{\mathbf{T}}, \qquad \tilde{\mathbf{B}} = \mathbf{T}\mathbf{B}, \qquad \tilde{\mathbf{C}} = \mathbf{C}\tilde{\mathbf{T}},$$

$$\tilde{\mathbf{A}} \in \mathrm{R}^{r\times r}, \qquad \tilde{\mathbf{B}} \in \mathrm{R}^{r\times m}, \qquad \tilde{\mathbf{C}} \in \mathrm{R}^{n\times r}.$$

2.2.2 Hybrid model reduction

In this dissertation, a model reduction method is proposed as a hybrid of nonlinear and linear model reduction techniques. As shown in [41]-[42], the transformation matrices $\mathbf{T}$ and $\tilde{\mathbf{T}}$ can be used to reduce the nonlinear system as well. In this case, the system can be represented as follows:

$$\begin{cases} \dot{\tilde{\mathbf{x}}} = \mathbf{T}\mathbf{f}\left(\tilde{\mathbf{T}}\tilde{\mathbf{x}}, \mathbf{u}\right) \\ \mathbf{y} = \tilde{\mathbf{T}}\tilde{\mathbf{x}} \end{cases} \tag{2.10}$$

The system in (2.10) has fewer states than the original system but it is still necessary to compute all nonlinear functions in **f**. Thus, there is basically no reduction in computation time. To address this problem, reference [43] suggests eliminating some of the functions. However, as it is shown in [44] it can create large errors due to the model reduction.

In the proposed hybrid model reduction approach, the functions that have the least contributions to the dynamics between the external area and a study area are not eliminated

but linearized. To evaluate contributions of the functions, let us consider the expressions for the d-axis current and the q-axis current of generators in the external area as these expressions have most nonlinearities and are used in 33 % of all differential equations in (2.1).

Nonlinearities in the expressions are cosine and sine functions and coefficients of these functions are conductances and susceptances between generators including fictitious generators representing the boundary between the external area and the study area. These values are real and imaginary parts of elements of the admittance matrix:

$$Y_{ij} = G_{ij} + jB_{ij}. \tag{2.11}$$

The matrix can be divided into four submatrices:

$$\mathbf{Y} = \begin{pmatrix} \mathbf{Y}_{11} & \mathbf{Y}_{12} \\ \mathbf{Y}_{21} & \mathbf{Y}_{22} \end{pmatrix}, \tag{2.12}$$

where $\mathbf{Y}_{11} \in \mathrm{R}^{N_g \times N_g}$ is the admittance matrix representing connections between generators inside the external area; $\mathbf{Y}_{22} \in \mathrm{R}^{N_b \times N_b}$ is the admittance matrix representing connections between fictitious generators; $\mathbf{Y}_{21} = \mathbf{Y}_{12}^T \in \mathrm{R}^{N_b \times N_g}$ is the admittance matrix representing connections between the generators of the external area and the fictitious generators.

Thus, column norms of absolute values of elements in matrix $\mathbf{Y}_{21}$ can be used to determine which function is to be linearized as the norms describe how close electrically each generator is to the boundary between the external area and a study area.

Column norms are calculated by:

$$\nu_i = \sqrt{\sum_{j=1}^{N_b} \left| Y_{21\,ji} \right|^2}. \tag{2.13}$$

The nonlinear functions that correspond to the generators with large column norms are kept nonlinear, and the nonlinear generator functions with small column norms are linearized. Thus, the hybrid reduced system can be represented as follows:

$$\begin{cases} \dot{\tilde{\mathbf{x}}} = \mathbf{T} \begin{pmatrix} \hat{\mathbf{f}}\left(\tilde{\mathbf{T}}\tilde{\mathbf{x}}, \mathbf{u}\right) \\ \mathbf{f}_l \end{pmatrix} \\ \mathbf{y} = \tilde{\mathbf{T}}\tilde{\mathbf{x}} \end{cases} \tag{2.14}$$

where $\mathbf{f}_l = \hat{\mathbf{A}}\Delta\tilde{\mathbf{x}} + \hat{\mathbf{B}}\Delta\mathbf{u} + \hat{\mathbf{x}}^0$, $\hat{\mathbf{A}} = \hat{\mathbf{P}}\mathbf{A}\tilde{\mathbf{T}}$, $\hat{\mathbf{B}} = \hat{\mathbf{P}}\mathbf{B}$, $\hat{\mathbf{A}} \in \mathrm{R}^{(n-q)\times r}$, $\hat{\mathbf{B}} \in \mathrm{R}^{(n-q)\times m}$, $\hat{\mathbf{x}}^0 = \hat{\mathbf{P}}\mathbf{x}^0$, vector $\hat{\mathbf{f}}$ comprises the functions that are kept nonlinear; $\mathbf{f}_l$ has the linearized functions; $\mathbf{x}^0$ is the initial state vector; $\hat{\mathbf{P}}$ is the identity matrix with deleted rows that correspond to the functions in $\hat{\mathbf{f}}$; q is the number of nonlinear functions in $\hat{\mathbf{f}}$.

The system in (2.14) can be rewritten as:

$$\begin{cases} \dot{\tilde{\mathbf{x}}} = \mathbf{T} \begin{pmatrix} \hat{\mathbf{f}}\left(\tilde{\mathbf{T}}\tilde{\mathbf{x}}, \mathbf{u}\right) \\ \hat{\mathbf{A}}\Delta\tilde{\mathbf{x}} + \hat{\mathbf{B}}\Delta\mathbf{u} + \hat{\mathbf{x}}^0 \end{pmatrix} \\ \mathbf{y} = \tilde{\mathbf{T}}\tilde{\mathbf{x}} \end{cases} \tag{2.15}$$

2.3 Adaptive Switching Algorithm

Considering that the linearly reduced system gives satisfactory performance during small disturbances, the duration of a large disturbance is short, and the majority of the time a system is under small or no disturbance it is reasonable to change the type of the model reduction of the external system to increase the accuracy and speed of the system

simulation. The proposed adaptive algorithm can adaptively change the complexity of the external area model based on the current condition as shown in Figure. 2.2

During the fault-on period, the original, fully detailed system model is used as the maximum accuracy of the system model is required and the duration of a fault is limited to tens of milliseconds, which only slightly increases the simulation time. To obtain the initial condition of the post-fault simulation the state vector from the last iteration of the fault-on simulation is multiplied by the transformation matrix. In the post-fault period, when the angle deviation $\Delta\delta_i$ of any generator in a study area exceeds a preset threshold $\Delta\delta_{\max}$, the external area is reduced using the hybrid model reduction method, which keeps the balance between accuracy and speed of simulation when the disturbance is large. In pre-fault and post-fault periods when all angle deviations are within the threshold, the external area is reduced using a linear model reduction method. This guarantees that most of the time when there is no disturbance or variation of the state is very small, the fastest model reduction method is applied.

To calculate the rotor angle deviation, the generator with the smallest column norm is used as a reference; i.e., the reference generator is the electrically farthest generator from a study area and has the least reactions to disturbances in study areas. If the time for a rotor angle deviation $\Delta\delta_i$ exceeding threshold, $\Delta\delta_{\max}$ denoted by, t_{th} is longer than a preset limit $t_{th_{\max}}$ a new operating condition is obtained and matrices $\tilde{\mathbf{A}}$ and $\tilde{\mathbf{B}}$ of the linearly reduced system are recalculated. This action corrects the adaptive algorithm after a large change of the system state. As the linearization is performed offline and the update is only

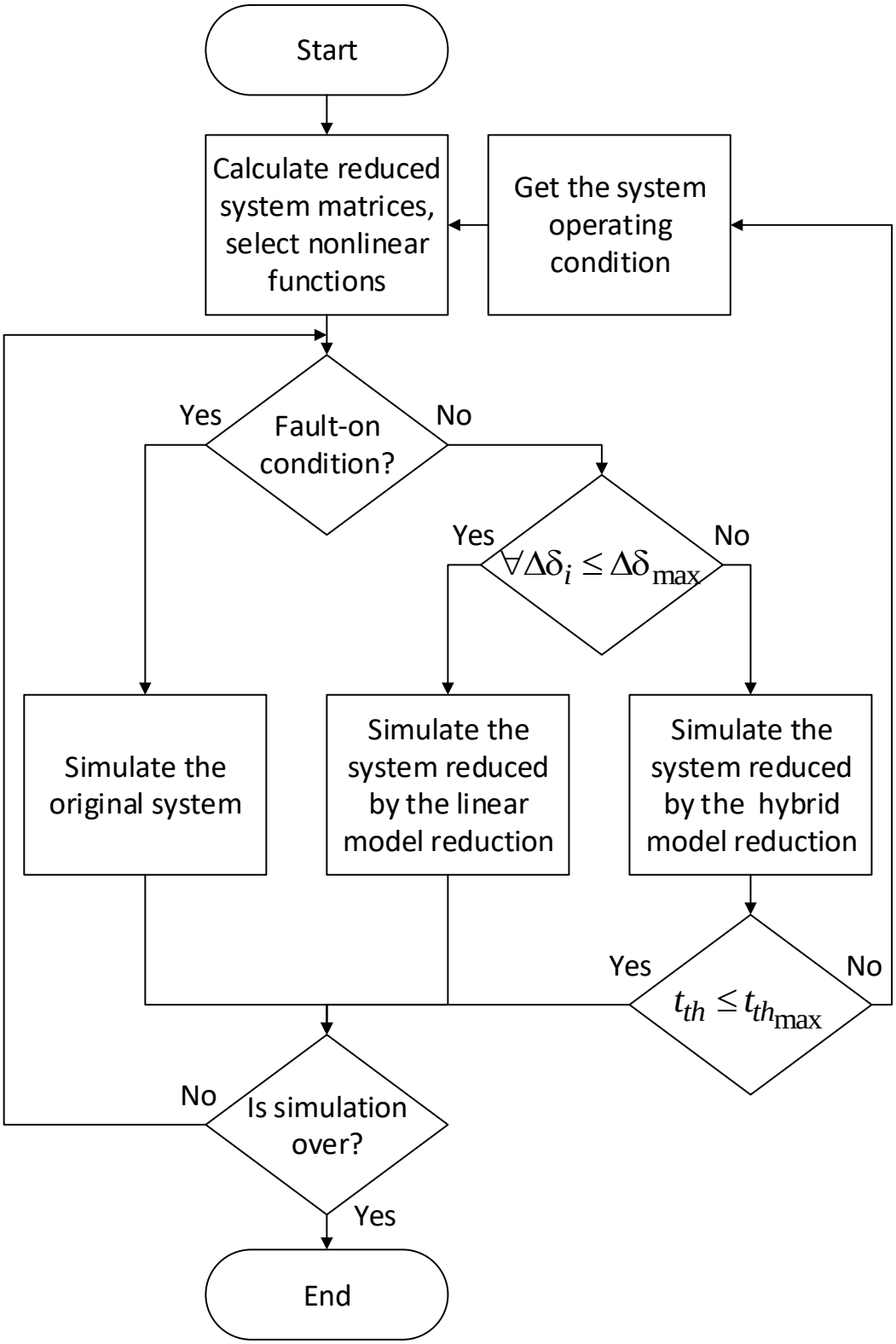

Figure 2.2. Adaptive switching algorithm.

necessary when a substantial change of the operating condition occur, the matrix recalculation does not affect the speed of the algorithm over a long period of time. Thus, the proposed approach is scalable to deal with large power system models.

2.4 Adaptive Model Reduction of the System without Partitioning

Partitioning the system into the study area and the external area creates a specific error. The error is caused by the fact that the inputs (boundary bus voltage magnitudes and boundary bus voltage angles) are calculated at the previous iteration of the simulation, i.e. the inputs are lagging by one iteration. To eliminate the partitioning error, the second version of the adaptive approach is proposed. This version is applied to the whole system that is treated as just one area.

Without the partitioning, there is no need in the concept of fictitious generators representing boundary buses of the study area and the external area, and the expressions in (2.1) for the d-axis current and the q-axis current are simplified as:

$$I_{d_i} = \sum_{j=1}^{N_g} E'_{d\,j} \left[G_{ij} \cos(\delta_i - \delta_j) + B_{ij} \sin(\delta_i - \delta_j) \right] + \sum_{j=1}^{N_g} E'_{q\,j} \left[G_{ij} \sin(\delta_i - \delta_j) - B_{ij} \cos(\delta_i - \delta_j) \right],$$

$$I_{q_i} = \sum_{j=1}^{N_g} E'_{d\,j} \left[-G_{ij} \sin(\delta_i - \delta_j) + B_{ij} \cos(\delta_i - \delta_j) \right] + \sum_{j=1}^{N_g} E'_{q\,j} \left[G_{ij} \cos(\delta_i - \delta_j) + B_{ij} \sin(\delta_i - \delta_j) \right].$$

As the single area of the system contains all generators including the generators from the study area whose dynamics are of the main interests, the transformation and truncation of the states are not performed, and the performance improvement comes only from the linearization of nonlinear functions. In the absence of inputs from the boundary

between the study area and the external area, the control matrix is eliminated from (2.15) and the system used in the second version of the adaptive approach is simplified as:

$$\begin{cases} \dot{\mathbf{x}} = \begin{pmatrix} \hat{\mathbf{f}}(\mathbf{x},\mathbf{u}) \\ \hat{\mathbf{A}}\Delta\mathbf{x} + \hat{\mathbf{x}}^0 \end{pmatrix} \\ \mathbf{y} = \mathbf{x} \end{cases} \tag{2.16}$$

where

$$\hat{\mathbf{A}} = \hat{P}A, \qquad \hat{\mathbf{A}} \in R^{(n-q)\times n}.$$

All nonlinear functions representing generators of the study area are contained in $\hat{\mathbf{f}}$. The list of linearized functions corresponding to generators of the external area is the same as in the adaptive approach applied to the partitioned system described above. The adaptive switching is performed between the system in (2.16) and the simplified version of the linearized system in (2.3):

$$\begin{cases} \Delta\dot{\mathbf{x}} = \mathbf{A}\Delta\mathbf{x} \\ \Delta\mathbf{y} = \mathbf{C}\Delta\mathbf{x} \end{cases} \tag{2.17}$$

As all generators of the system including those of the study area are linearized in (2.17) the angle deviation threshold $\Delta\delta_{\max}$ of the adaptive switching algorithm is set to a small value to enable switching when large oscillations are damped.

2.5 Case Studies

Comprehensive case studies are conducted to compare the proposed adaptive model reduction approaches with the traditional linear model reduction approach. A realistic power system model is tested. For the system, the study area is defined and retained with original, detailed models, and the rest of the system is defined as the external area to be

reduced respectively by different approaches. Then, time-domain contingency simulation using each reduced system model is conducted and compared with the simulation using the original system model. In addition, the approaches are validated during different post-fault operating conditions and compared with the traditional coherency-based model reduction approach.

2.5.1 Temporary bus fault tests

The linear model reduction approach and the adaptive approaches described above are applied to the NPCC 140-bus 48-generator system shown in Figure 2.3. The study area is set to be the ISO-NE region having 9 generators. The external area is set to be the rest of the system, which has 39 generators, 39×9=351 state variables and 39×4=156 nonlinear functions since the first 5 state variables of each generator is described by linear differential equations. The external area is connected to the study area by two tie-lines.

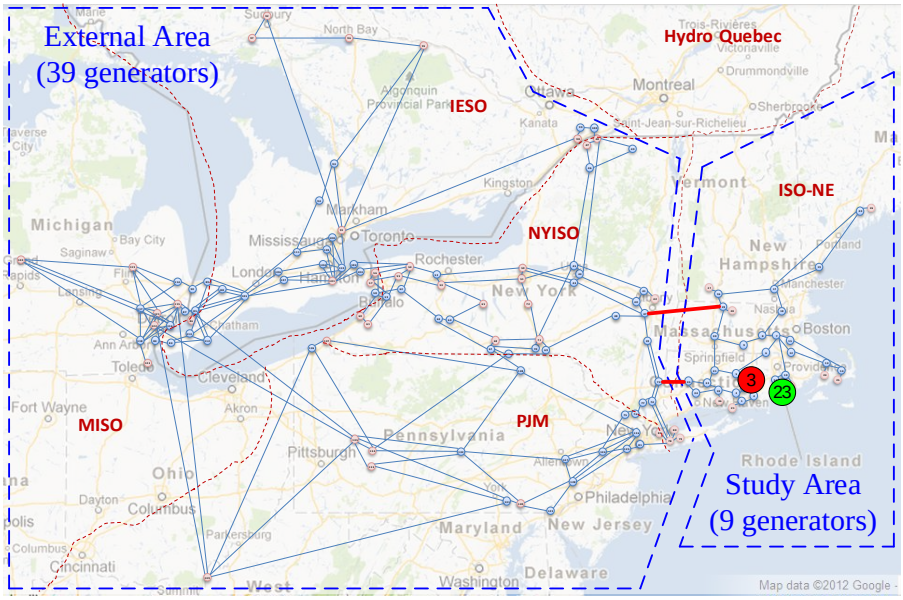

Figure 2.3. Partitioned NPCC system.

The H_∞ norm of the balanced truncation error is set to be equal to 10^{-5}:

$$10^{-5} \le 2 \sum_{i=r+1}^{n} \sigma_i. \tag{2.18}$$

This corresponds to truncating 200 out of 351 state variables. To find the threshold value of the column norm of the admittance matrix that decides if generator is electrically close to the boundary, a case study is performed on the system in (2.15). The threshold decreases with 0.1-p.u. increments from 10 until all rotor angle errors following any of the contingencies are below 6 degrees. After the case study, the threshold is set as 1 p.u. Nonlinear functions corresponding to generators with column norms of the admittance matrix less than 1.0 p.u. are linearized. This corresponds to linearization of 136 out of 156 nonlinear functions of the external area in the case of partitioned system and 136 out of 192 nonlinear functions of the unpartitioned system.

The column norm threshold per unit value in not useful if the proposed approach is applied to a system with a different base power. To make it more practical, it is converted to a value in siemens. The NPCC system has the base power of 100 MVA. Setting the base voltage to the common generator terminal voltage of 20 kV the new thresholds is calculated:

$$Y_{th} = 1\frac{S_{base}}{V_{base}^2} = 1\frac{100\times10^6}{\left(20\times10^3\right)^2} = 0.25S. \tag{2.19}$$

When the proposed approach is applied to a different system, the threshold is converted to a per unit value using the new system MVA base and the base voltage of 20 kV.

Another case study is performed to select the angle deviation threshold $\Delta\delta_{max}$ for the adaptive switching algorithm applied to the partitioned system. The threshold is decreased with 1-degree increments from 180 degrees until all rotor angle errors for all generators following any of the contingencies are below 6 degrees. After this case study, $\Delta\delta_{max}$ is set to 67 degrees. The threshold for the adaptive approach applied to the unpartitioned system is set to 6 degrees to ensure that the rotor angle errors of generators representing study area are also below 6 degrees.

The simulations are performed in MATLAB R2015a on a computer with a 4-GHz AMD FX-8350 processor and 8 GB of memory. The duration of the simulation is set to 16 seconds with an integration time step of 0.01 seconds.

To compare the approach performance during a large disturbance, a three-phase short circuit fault lasting for the critical clearing time (CCT) is created separately at every bus of the study area. CCT is calculated using the original system, CCTs of the adaptively reduced systems are the same as the ones of the original system, CCTs of the linearly reduced system are smaller or equal to the ones of the original system. The errors of all outputs (state variables) of all generators in the study area are analyzed and the rotor angle state variable has the largest error for each of the generators. For every fault, the generator with the largest error of the rotor angle is found and used to compare the approaches. The results of comparison of rotor angle root mean square errors of the linear model reduction and the adaptive approaches are shown in Table 2.1. From Table 2.1, the linear model reduction approach cannot guarantee satisfactory performance during large disturbances

Table 2.1. Comparison of RMS Error of Rotor Angle

Bus	Generator	CCT	Partitioned		Unpartitioned
			Linear	Adaptive	Adaptive
1	26	0.13	8.85	1.33	1.06
2	26	0.13	3.10	0.86	0.57
3	23	0.39	25.94	5.51	5.12
4	26	0.12	1.50	0.75	0.41
5	23	0.09	0.59	0.48	0.29
6	23	0.08	0.72	0.60	0.30
7	26	0.05	0.28	0.28	0.47
8	23	0.05	4.87	4.41	0.29
9	26	0.06	3.26	2.83	0.29
10	26	0.13	10.49	2.90	1.26
11	23	0.19	8.81	1.40	1.46
12	23	0.1	1.89	0.98	0.44
13	23	0.12	2.57	0.97	0.49
14	23	0.13	2.83	1.00	0.51
15	23	0.07	0.38	0.38	0.33
16	23	0.05	0.87	0.78	0.31
17	26	0.03	0.30	0.30	0.59
18	23	0.04	0.33	0.33	0.66
19	26	0.03	0.11	0.11	0.95
20	26	0.03	0.27	0.27	1.05
21	23	0.22	12.97	1.65	1.89
22	23	0.19	6.55	1.32	1.06
23	23	0.20	3.83	1.07	0.71
24	23	0.18	5.66	1.46	0.91
25	23	0.22	20.45	2.22	3.87
26	26	0.03	0.35	0.34	0.86
27	23	0.10	0.29	0.27	0.46
28	26	0.12	0.28	0.30	0.42
29	23	0.06	3.15	3.48	0.43
30	23	0.06	1.21	1.35	0.38
31	23	0.08	0.40	0.43	0.25
32	26	0.11	1.25	0.79	0.42
33	26	0.11	1.05	0.65	0.39
34	23	0.15	3.79	0.89	0.63
35	26	0.14	3.14	0.82	0.52
36	23	0.21	4.03	0.92	0.61

generating errors of more than 25 degrees while the proposed adaptive approach keeps the error for all disturbances within 6 degrees both for the case with the system partitioned into a study area and external area and the case with only one area representing the whole system.

The fault at bus 3 is the largest disturbance of the NPCC system, and generator 23 has the largest rotor angle error following this fault, and thus its rotor angle is used for the comparison. The results of the simulation are shown in Figure 2.4 when the adaptive approach is applied to the partitioned system and in Figure 2.5 when the adaptive approach is applied to unpartitioned system.

As it can be seen from Figure 2.4 and Figure 2.5, if the external system is reduced using linear model reduction, the rotor angle trajectory differs significantly from the rotor angle trajectory of the original system whereas the rotor angle trajectory of the system reduced by the adaptive approaches follows accurately the original trajectory.

To present in more detail the difference between approaches, the root mean square errors of all state variables are calculated using the following expression:

$$\varepsilon_i = \sqrt{\frac{\sum_{j=1}^{N} \left(x_{ij} - \hat{x}_{ij} \right)^2}{N}}, \tag{2.20}$$

where N is the number of simulation steps; x_{ij} and $\hat{x}_{ij}$ are respectively the values of i-th state variable of generator 23 of the original system and the reduced system at time step j. The results of this calculation are shown in Table 2.2. The proposed adaptive approaches reduce the error by 74% to 81% for every state variable compared to the linear model reduction approach.

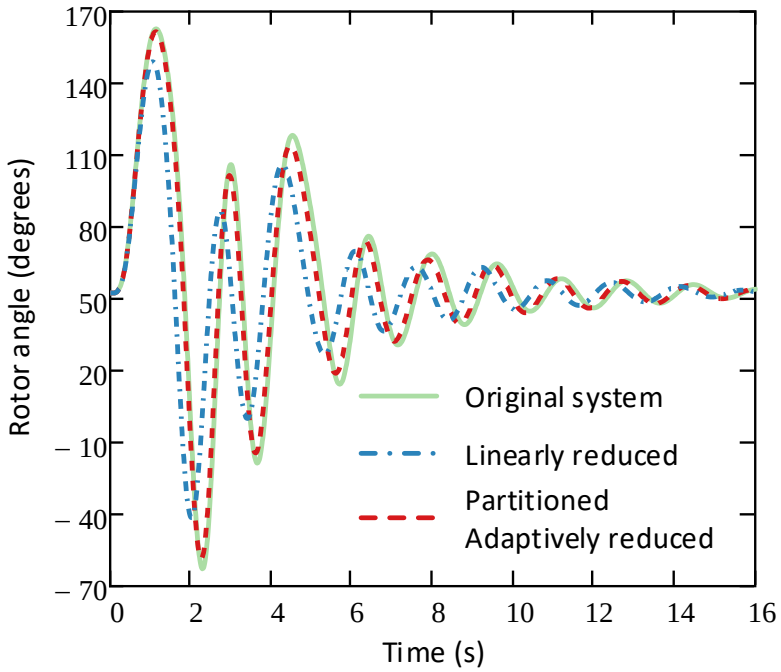

Figure 2.4. Rotor angle of generator 23 following the fault at bus 3 including the partitioned system.

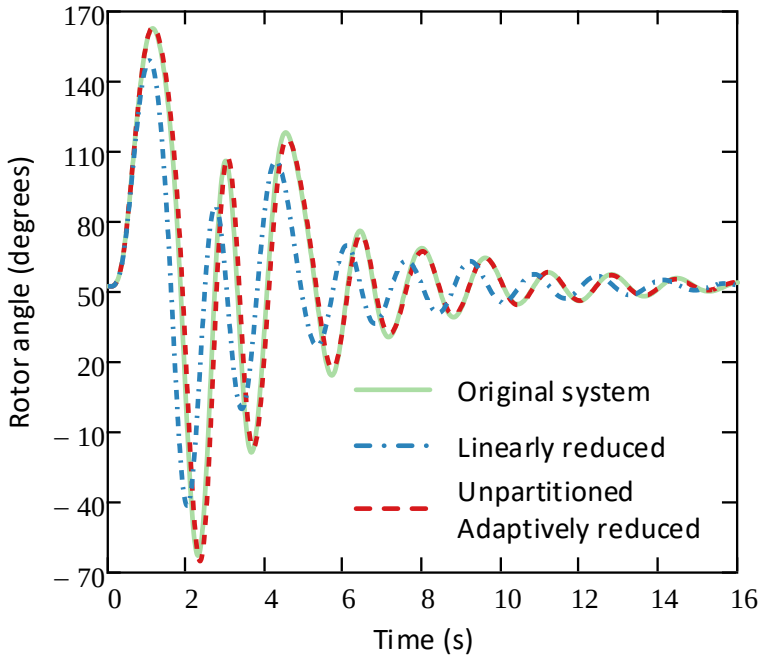

Figure 2.5. Rotor angle of generator 23 following the fault at bus 3 including the unpartitioned system.

A fault with the duration equal to CCT is the worst-case scenario that can cause the largest error. The worst-case errors of the proposed adaptive model reduction approach are small enough to justify its applicability to power system stability studies.

In addition to accuracy, the approaches are compared in terms of simulation time as shown in Table 2.3.

In Table 2.3 the large disturbance corresponds to the 0.39-second fault at bus 3 and the small disturbance corresponds to the 0.03-second fault at bus 17. The results show that the proposed adaptive approach applied to the partitioned system reduces the simulation time by 57% during the large disturbance and by 59% during the small disturbance compared to the original system. If the adaptive approach is applied to the unpartitioned system, the simulation time is reduced by 73% and 84% respectively for the small disturbance and the large disturbance. The difference in simulation time between two versions of the adaptive approach is caused by the transformation and partitioning in the partitioned system and by the fact that the whole unpartitioned system is switched to the linearized model which is the fastest model. Especially it is clear in the case of the small disturbance as the switching to the linear model happens earlier.

Thus, the proposed adaptive approach provides both high accuracy and high simulation speed.

2.5.2 Test of operating condition change

To test the robustness of the adaptive approach against a change of the operating condition, the temporary fault at bus 3 representing the largest disturbance is changed to a

Table 2.2. Comparison of RMS Error of States of Generator 23

States	System		
	Linearly reduced	**Partitioned adaptively reduced**	**Unpartitioned adaptively reduced**
δ, degrees	2.24×10^{1}	5.5×10^{0}	5.1×10^{0}
P_m, p.u.	1.8×10^{-3}	4.1×10^{-4}	3.4×10^{-4}
P_{gv}, p.u.	2.3×10^{-2}	5.1×10^{-3}	4.5×10^{-3}
V_R, p.u.	1.7×10^{-1}	3.7×10^{-2}	4.1×10^{-2}
R_f, p.u.	1.3×10^{-2}	3.4×10^{-3}	3.2×10^{-3}
E_{fd}, p.u	9.8×10^{-2}	2.2×10^{-2}	2.3×10^{-2}
E'_d, p.u.	6.9×10^{-2}	1.4×10^{-2}	1.5×10^{-2}
E'_q, p.u.	1.1×10^{-2}	2.8×10^{-3}	2.6×10^{-3}
ω, p.u.	4.7×10^{-3}	1.0×10^{-3}	9.7×10^{-4}

Table 2.3. Comparison of Simulation Time

System	Simulation time, seconds	
	Large disturbance	**Small disturbance**
Original unpartitioned	3.7	
Partitioned and linearly reduced	0.9	
Partitioned and adaptively reduced	1.6	1.5
Unpartitioned and adaptively reduced	1.0	0.6

permanent fault cleared by tripping one of the lines connected to the bus or by completely isolating the bus by tripping all lines connected. Following the bus fault, the operating condition of the system is changed. The results of simulation are shown in Table 2.4.

Table 2.4 shows that the proposed adaptive approach can reduce the system after the change of the operating condition maintaining the accuracy of simulation.

2.5.3 Comparison with the coherency-based model reduction

Proposed adaptive approaches are compared to another traditional model reduction approach based on grouping coherent generators following a small disturbance, which follows a conventional industry practice in coherency-based model reduction using commercialized software tools SSAT and DYNRED by Powertech Labs. First, the complete eigenvalue analysis is performed in SSAT. Accordingly, three dominant inter-area modes of oscillations between the study and the external area with the largest participation factors of generators of the study area are selected. The frequencies of the selected modes are 0.71 Hz, 0.72 Hz, and 0.77 Hz. Feed the SSAT result into DYNRED and use a tolerance-based method for generator grouping. Then, 17 groups of coherent generators are identified based on the selected modes. The first group of 9 generators correspond to the study area and the other 16 groups represent generators of the external area. The first group plus neighboring 36 buses are set to be the study area. Model reduction by DYNRED aggregates 39 generators of the external area into 16 equivalent generators resulting in a reduced 82-bus 25-generator system.

First, the proposed and traditional approaches are tested using faults at boundary buses. The results of the simulation are shown in Table 2.5 All approaches provide

satisfactory performance. The larger error of the partitioned systems is due to the larger partitioning error during contingencies at the boundary. The largest disturbance (0.39-second fault at bus 3) in the study area makes the coherency-based reduced system unstable. To compare the approaches, the duration of the fault is reduced to 0.38 seconds. The simulation results are shown in Table 2.6. Both traditional linear and coherency-based approaches provide similar performance in terms of accuracy and speed; however, the accuracy of proposed approaches is substantially higher.

2.6 Conclusions

This chapter has proposed two versions of a new adaptive model reduction approach that can be applied to traditional partitioned system or to unpartitioned system for fast power system simulation. The approach is capable of accurate representation of the original power system model with significant reduction in computational time. The adaptive approach has been comparted with the traditional coherency-based and linear model reduction approaches. The proposed approach provides substantial improvement in accuracy compared to the traditional approaches. In addition, the robustness of the approach to a change in operating condition has been confirmed.

Table 2.4. Comparison of Faults Leading to a New Operating Condition

Fault	Rotor angle RMS error, degrees	
	Partitioned adaptively reduced	**Unpartitioned adaptively reduced**
Temporary fault at bus 3	5.51	5.12
Fault at line 3-2 followed by the line trip	5.48	5.09
Fault at line 3-4 followed by the line trip	5.28	4.80
Fault at bus 3 followed by the bus trip	2.74	2.04

Table 2.5. Comparison of Model Reduction Approaches During Boundary Bus Faults

Fault	Rotor angle RMS error, degrees	
	Bus 29 fault	**Bus 35 fault**
Coherency-based reduced	0.93	2.27
Partitioned and linearly reduced	3.15	3.14
Partitioned and adaptively reduced	3.48	0.82
Unpartitioned and adaptively reduced	0.43	0.52

Table 2.6. Comparison of Model Reduction Approaches During Bus 3 Fault

System	Rotor angle RMS error, degrees	Simulation time, seconds
Coherency-based reduced	16.98	1.1
Partitioned and linearly reduced	14.14	0.9
Partitioned and adaptively reduced	2.30	1.6
Unpartitioned and adaptively reduced	1.96	1.0

CHAPTER THREE

APPLICATION OF ADAPTIVE MODEL REDUCTION WITH PARALLELISM IN SPACE

3.1 Power System Partitioning

As it was mentioned in chapter one, in power system model reduction the system is divided into two areas: 1) the study area, which is the main interest of an investigator, where all details are preserved and disturbances are originated from; 2) the external area, which can be simplified and reduced. In general, the reduced external area requires less time to simulate compare to the study area. Considering this fact, the study area can be further partitioned into multiple subareas which are simulated in parallel to decrease the total system simulation time. The partitioned power system with multiple study areas is shown in Figure 3.1.

Each area of the original system is connected to other areas by several tie-lines. For every area, each tie-line is treated as a fictitious generator with the internal voltage phasor equal to the voltage phasor of the corresponding boundary bus in the opposite area and with the armature resistance and transient reactance equal to the resistance and reactance of the corresponding tie-line. These fictitious generators are treated as constant voltage sources during each iteration and represent the electrical power injections from one area to the other areas. Therefore, voltage magnitudes and voltage angles of boundary buses in one

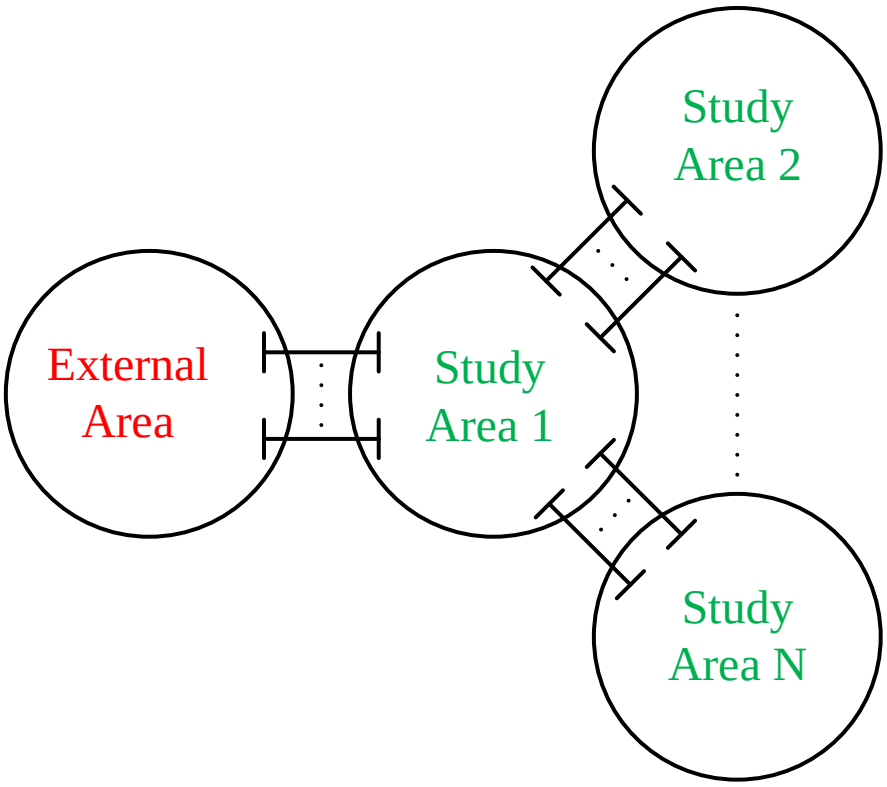

Figure 3.1. Partitioned power system with multiple study areas.

area are the inputs to the model of the other areas. At every iteration of the system simulation, each area is calculated separately, then boundary bus voltages of all areas are recalculated, and their values are sent as inputs to the corresponding areas to perform the next iteration. The simulation of each area can be done in parallel to decrease the total time of the simulation.

In this section, a power system is modeled based on the following assumptions: 1) loads are represented by constant admittances, 2) network nodes are eliminated [40], 3) sub-transient dynamics and saturation are ignored, 4) torque in p.u. is equal to mechanical power in p.u., 5) damper windings' time constants are equal to zero, 6) synchronous reactances are equal to transient reactances, 7) an exciter with one gain and one time

constant is used for each generator, 8) a governor with one time constant is used for each generator.

In each area of the partitioned system, every generator is described by the following five differential equations:

$$\begin{cases} \dot{\delta}_i = \omega_{base}\left(\omega_i - 1\right) \\ T'_{do_i}\dot{E}'_{q_i} = -E'_{q_i} + E_{fd_i} \\ T_{A_i}\dot{E}_{fd_i} = -E_{fd_i} + K_{A_i}\left(V_{ref_i} - V_{t_i}\right) \\ T_{gv_i}\dot{P}_{m_i} = -P_{m_i} + P_{ref_i} - \left(\omega_i - 1\right)/R_i \\ 2H_i\dot{\omega}_i = P_{m_i} - P_{e_i} - D_i\left(\omega_i - 1\right) \end{cases} \tag{3.1}$$

where

$$P_{e_i} = E'_{q_i}\sum_{j=1}^{N_g} E'_{q_j}\left[G_{ij}\cos(\delta_i - \delta_j) + B_{ij}\sin(\delta_i - \delta_j)\right]$$

$$+\ E'_{q_i}\sum_{j=1}^{N_b} V_j\left[G_{ij}\cos(\delta_i - \theta_j) + B_{ij}\sin(\delta_i - \theta_j)\right],$$

An example of transformation of the original system to the partitioned system with two study areas is shown in Figure 3.2. Voltage phasors of boundary buses in the external area $V_1^e\angle\theta_1^e$, $V_2^e\angle\theta_2^e$ and in the second study area $V_1^2\angle\theta_1^2$, $V_2^2\angle\theta_2^2$ are the internal voltage phasors of the fictitious generators of the first study area. Voltage phasors of boundary buses in the first study area $V_1^1\angle\theta_1^1$, $V_2^1\angle\theta_2^1$, $V_3^1\angle\theta_3^1$, $V_4^1\angle\theta_4^1$ are the internal voltage phasors of the fictitious generators of the external area and the second study area.

3.2 Case Studies

3.2.1 Temporary bus fault tests

The partitioning scheme described above together with the adaptive approach introduced in chapter two is tested on the NPCC system. The study area is set to be the New England region of the NPCC system, which has 9 generators. To test cases with multiple study areas, the study area is divided into two subareas: study area 1 with 5 generators and study area 2 with 4 generators. The external area is set to be the rest of the system, which has the other 39 generators. The external area has 39×5=195 state variables and 39 nonlinear functions as the first 4 states of each generator is described by linear differential equations. The external area is connected to study area 1 by two tie-lines, and study area 1 is connected to study area 2 by two tie-lines as shown in Figure 3.2. The partitioned NPCC system is shown in Figure 3.3.

The H_∞ norm of the balanced truncation error is set to be equal to 10^{-5}. This corresponds to truncation of 107 out of 195 state variables. The functions corresponding to column norms of admittance matrix less than 1.0 p.u. are linearized. This corresponds to linearization of 34 out of 39 functions. The angle deviation threshold $\Delta\delta_{\max}$ is set to 67 degrees. The simulation is performed for 16 seconds to represent at least 10 cycles of oscillations. The integration time step is set to 0.01 seconds.

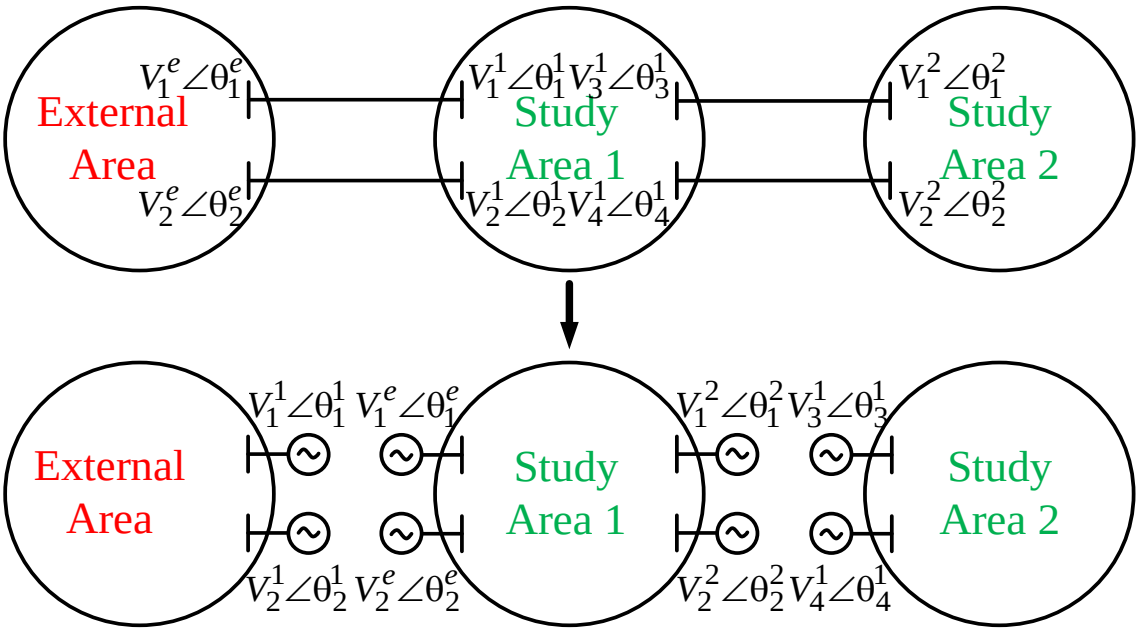

Figure 3.2. Transformation from the original system to the partitioned system.

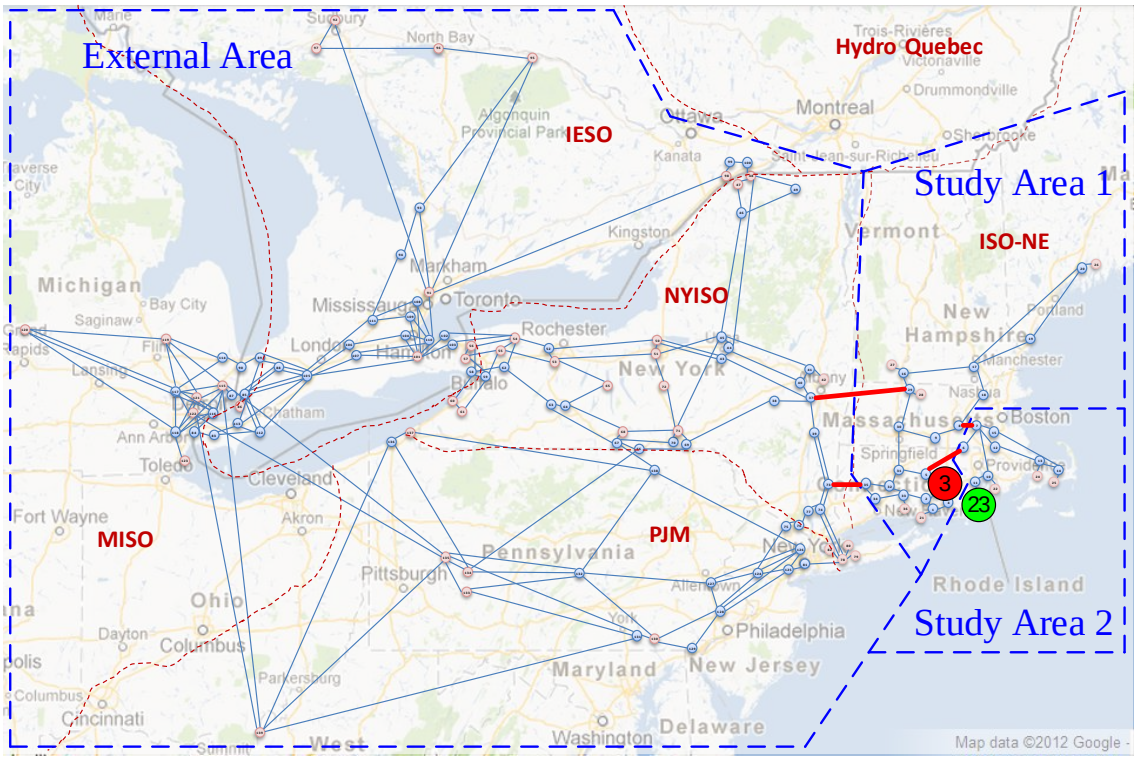

Figure 3.3. Partitioned NPCC system with multiple study areas.

To compare the approach performance during a large disturbance, a three-phase short circuit fault lasting for the critical clearing time (CCT) is created separately at every bus of the study areas. The error of all outputs (state variables) of all generators in the study areas are analyzed, and the rotor angle variable has the largest error for each of the generator. For every fault, the generator with the largest error of the rotor angle is found and used to compare the approaches. The results of comparison of rotor angle RMS errors of the linear model reduction approach and the adaptive approach are shown in Table 3.1. As Table 3.1 shows, the linear model reduction approach cannot guarantee satisfactory performance during large disturbances generating the errors of more than 30 degrees while the proposed adaptive approach keeps the error for all disturbances within 4 degrees both for the case with one study area and the case with two study areas including faults at the boundary buses.

The fault at bus 3 is the largest disturbance of the NPCC system, and generator 23 has the largest rotor angle error following this fault, and thus its rotor angle is used for comparison. The results of simulation are shown in Figure 3.4. As it can be seen from Figure 3.4, if the external system is reduced using linear model reduction, the rotor angle trajectory differs significantly from the rotor angle trajectory of the original system whereas the rotor angle trajectory of the system reduced by the adaptive approach follows accurately the original trajectory.

To present quantitatively the difference between approaches, the RMS errors of all states are calculated, and the results of calculation are shown in Table 3.2.

Table 3.1. Comparison of RMS Error of Rotor Angle Including the Case of Two Study Areas

Bus	Generator	CCT	1 study area		2 study areas
			Linear	Adaptive	Adaptive
1	26	0.22	17.84	1.05	0.97
2	26	0.22	8.09	0.90	0.89
3	23	0.67	33.20	3.35	3.82
4	26	0.22	14.19	0.97	1.23
5	23	0.14	1.24	0.37	0.57
6	23	0.11	0.64	0.28	0.49
7	26	0.07	1.26	1.07	1.37
8	23	0.06	0.21	0.12	0.26
9	26	0.08	0.76	0.85	1.27
10	26	0.21	14.24	0.90	1.59
11	23	0.29	27.47	1.75	3.35
12	23	0.15	2.02	0.55	1.53
13	23	0.2	6.39	0.96	1.23
14	23	0.23	29.43	2.27	2.08
15	23	0.11	1.18	0.38	3.40
16	23	0.07	0.16	0.13	0.25
17	26	0.04	0.08	0.07	0.30
18	23	0.05	0.10	0.07	0.12
19	26	0.04	0.05	0.04	0.13
20	26	0.04	0.08	0.07	0.24
21	23	0.28	5.66	0.76	0.85
22	23	0.28	10.58	1.02	1.03
23	23	0.26	4.06	0.82	0.93
24	23	0.27	14.29	1.02	1.23
25	23	0.29	10.96	0.97	1.06
26	26	0.04	0.08	0.07	0.24
27	23	0.15	0.36	0.19	0.24
28	26	0.21	2.39	0.51	0.55
29	23	0.08	0.41	0.19	0.31
30	23	0.08	0.39	0.18	0.33
31	23	0.12	0.79	0.30	0.40
32	26	0.19	11.53	0.97	2.85
33	26	0.19	6.42	0.89	1.13
34	23	0.26	14.32	1.20	1.20
35	26	0.25	24.52	1.65	2.55
36	23	0.27	9.41	1.13	0.94

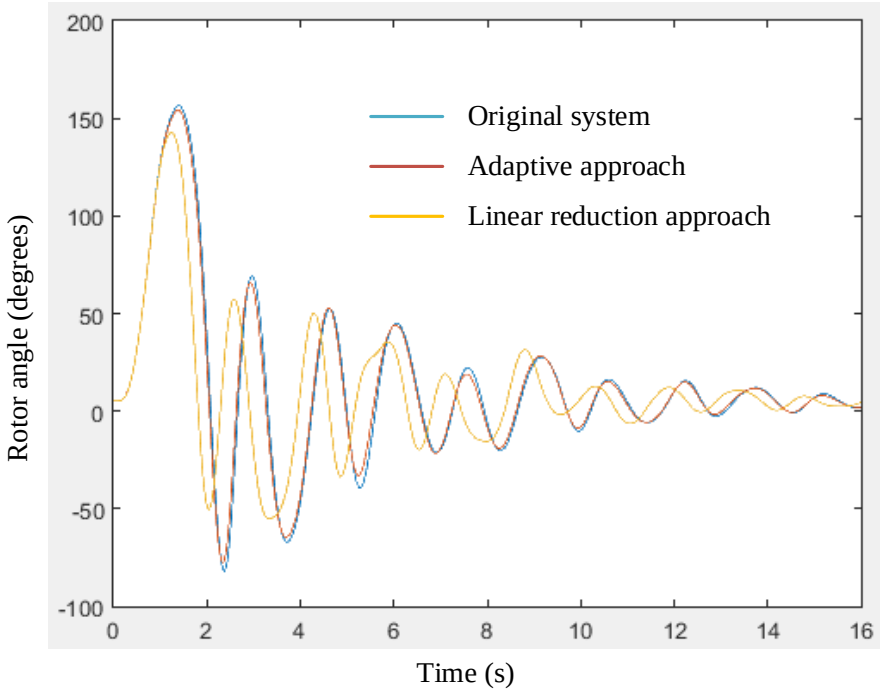

Figure 3.4. Rotor angle of generator 23 following the fault at bus 3.

Table 3.2. Comparison of RMS Error of States of Generator 23 Including the Multiple Areas Case

States		**System**		
		Only partitioned	**Linearly reduced**	**Adaptively reduced**
δ, rad	1 study area	1.4×10^{-3}	5.8×10^{-1}	5.9×10^{-2}
	2 study areas	9.1×10^{-2}	5.9×10^{-1}	6.7×10^{-2}
E'_q, p.u.	1 study area	2.3×10^{-5}	9.3×10^{-3}	1.0×10^{-3}
	2 study areas	1.4×10^{-3}	9.5×10^{-3}	1.2×10^{-3}
E_{fd}, p.u	1 study area	3.4×10^{-4}	1.5×10^{-1}	1.5×10^{-2}
	2 study areas	2.4×10^{-2}	1.5×10^{-1}	1.7×10^{-2}
P_m, p.u.	1 study area	3.5×10^{-4}	1.5×10^{-1}	1.5×10^{-2}
	2 study areas	2.3×10^{-2}	1.5×10^{-1}	1.7×10^{-2}
ω, p.u.	1 study area	1.5×10^{-5}	6.9×10^{-3}	6.9×10^{-4}
	2 study areas	1.1×10^{-3}	7.0×10^{-3}	7.9×10^{-4}

The proposed adaptive approach reduces the error by 87 % to 90 % for every state variable compared to the linear model reduction approach. And for the case with two study areas, the adaptive approach is more accurate than the approach with only partitioning the system since the adaptive approach switches to the original unpartitioned system during a fault. The error of the only partitioned system is caused by the fact that the inputs (voltage phasors of the boundary buses) are calculated at the previous iteration of the simulation, i.e. the inputs are lagging by one iteration.

A fault with the duration equal to CCT is the worst-case scenario that can cause the largest error. The proposed approach has the worst-case error of 4 degrees, which justifies its application in power system stability studies.

In addition to accuracy, the approaches are compared in terms of simulation time as shown in Table 3.3. The results show that the proposed adaptive approach applied to the partitioned system with one study area reduces the simulation time by 51% compared to the original system.

If the system with two study areas is used, the simulation takes more time to complete. However, if simulations of multiple areas can be performed in parallel, the case with multiple study areas performs even faster than the case with only one study area. This can be seen from the Table 3.4, which decomposes simulation time into areas.

The difference between linearly and adaptively reduced systems in terms of simulation time of the study areas and the rest of the simulation is caused by the fact that during the fault the adaptive approach switches to the original system and this stage cannot be parallelized and its simulation time is accounted as the rest of the simulation.

Table 3.3. Comparison of Simulation Time Including the Multiple Areas Case

System	Simulation time, seconds	
	1 study area	2 study areas
Original	11.9	
Only partitioned	12.7	14.5
Partitioned and linearly reduced	5.3	7.1
Partitioned and adaptively reduced	5.8	7.5

Table 3.4. Decomposition of Simulation Time in the Parallel Mode

Components		System simulation time, seconds			
		Original	Partitioned	Linearly reduced	Adaptively reduced
1 study area	Study	11.9	2.6		2.5
	External		8.4	1	1.5
	The rest		1.7		1.8
	Total		10.1	4.3	4.3
2 study areas	Study 1		2.2		2.1
	Study 2		2.2		2.1
	External		8.4	1	1.5
	The rest		1.7		1.8
	Total		10.1	3.9	3.9

Table 3.4 shows that in the parallel mode of simulation the adaptive approach time performance is identical to the linear model reduction approach, and the approach reduces the simulation time by 67 % compared to the original system.

Thus, the proposed adaptive approach with multiple study areas provides both high accuracy and high simulation speed.

3.2.2 Test of operating condition change

To test how the adaptive approach performs robustly against a change of the operating condition, the temporary fault at bus 3 is changed to a permanent fault cleared by isolation of the bus by tripping all lines connected. Following that contingency, the operating condition of the system is changed.

The results of simulation are shown in Table 3.5. Table 3.5 shows that the proposed adaptive approach maintains the accuracy of the reduced model after the change of the operating condition.

3.2.3 Test of slow mode of oscillation

To verify that slow modes of oscillations are preserved when the adaptive approach is applied, the slowest mode at 0.266 Hz is excited using the technique described in [45]. The results of the simulation are shown in Figure 3.5.

The difference between the original system and the adaptively reduced system is caused by the fact that in order to excite a specific mode, not only rotor angles of the generators in the study areas but also rotor angles of the generators in the external area are

changed. This violates the assumption that all disturbances are originated from the study areas. However, even in this condition the adaptive approach performs satisfactorily.

To test the adaptive approach, Prony analysis of the frequency of the generator 23 was performed. The results of the analysis are shown in Table 3.6, from which the proposed adaptive approach preserves the modal properties of the slowest oscillation mode.

3.3 Conclusions

This chapter has proposed a power system partitioning approached with multiple study areas calculated in parallel for fast power system simulation. The approach is capable of accurate representation of the original power system model with significant reduction in computational time. The approach has been compared with the traditional linear model reduction approach and maintains better accuracy even when there is a change in operating condition. In addition, it has been shown that the proposed approach preserves the slow inter-area mode of oscillations.

Table 3.5. Comparison of Faults Leading to a New Operating Condition Including the Multiple Areas Case

Fault	Rotor angle RMS error, degrees	
	1 study area	2 study areas
Temporary fault at bus 3	3.35	3.82
Fault at line 3-2 followed by the line trip	3.34	3.81
Fault at line 3-4 followed by the line trip	3.29	3.76
Fault at bus 3 followed by the bus trip	2.25	2.60

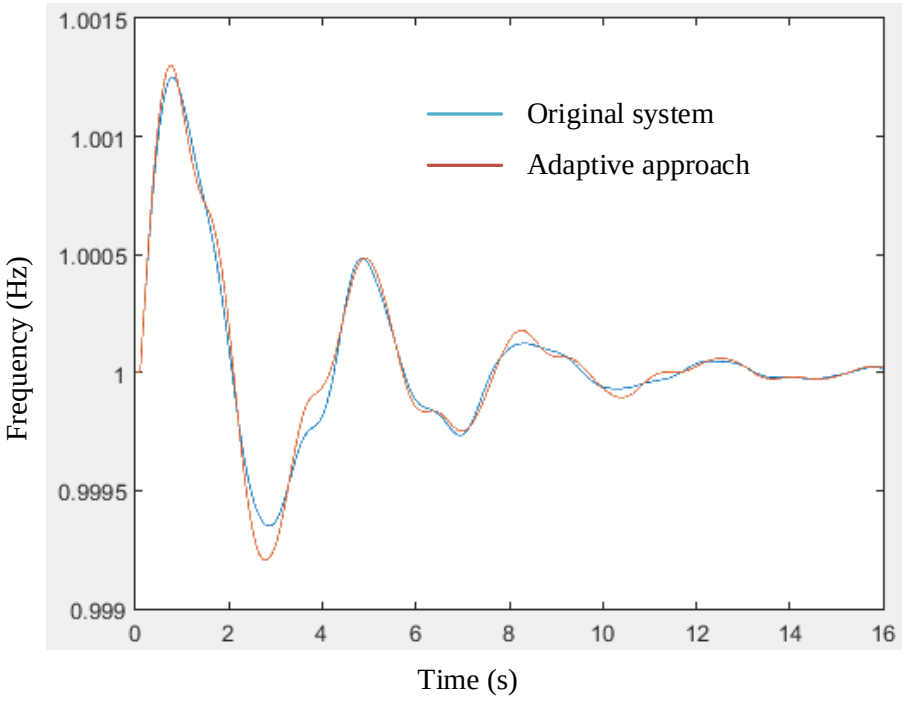

Figure 3.5. Frequency of generator 23 after 0.266-Hz mode is excited.

Table 3.6. Slowest Oscillation Mode Comparison

System		Amplitude, p.u.	Frequency, Hz	Damping, %
Original		0.015	0.266	16.8
Adaptively reduced	1 study area	0.016	0.266	16.3
	2 study areas	0.015	0.266	16.2

CHAPTER FOUR

APPLICATION OF ADAPTIVE MODEL REDUCTION WITH PARALLELISM IN TIME

The adaptive model reduction described in chapter two can be used together with the Parareal method improving the speed of the coarse solver and decreasing the total simulation time. In the Parareal method the simulation time is divided into subintervals with a coarse time step. Each interval is then simulated in parallel using a fine solver. Based on the fine solution of each interval the coarse solution propagated by a coarse solver is then corrected. The concept of Parareal method is show in Figure 4.1. There are two main Parareal algorithms: the master-workers algorithm and the distributed algorithm [46].

In the master-workers algorithm the initial coarse solution propagation is performed by the master processor and the results are sent to the worker processors to propagate the fine solutions. The fine solutions are then sent back to the master processor where the coarse solution is propagated and corrected. This algorithm is suited for shared memory systems [47], where all processors share the same global memory. In the distributed algorithm the coarse propagation and correction are distributed across all processors. This algorithm is suited for distributed memory systems (message passing systems) [47], where each processor uses its own local memory.

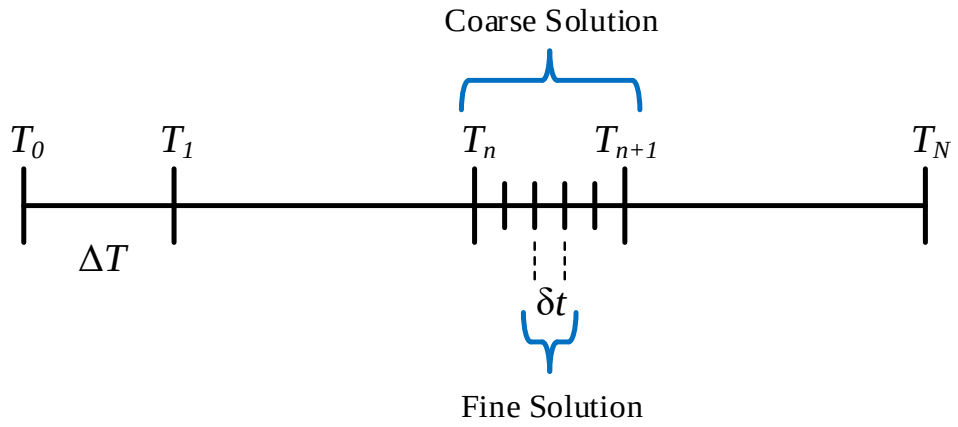

Figure 4.1. Parareal method.

4.1 Master-Workers Algorithm

4.1.1 Parareal algorithm

At the beginning of the master-workers Parareal algorithm, an initial guess of the coarse solution needs to be propagated using the coarse solver $C_{\Delta T}$,

$$\begin{aligned} &\mathbf{U}_n^0 = \tilde{\mathbf{U}}_n^0 = C_{\Delta T}(\mathbf{U}_{n-1}^0), \quad \forall 1 \le n < N_c, \\ &\mathbf{U}_0^1 = \mathbf{U}_0^0, \end{aligned} \tag{4.1}$$

where $\tilde{\mathbf{U}}_n$ and $\mathbf{U}_n$ represent the vector of state variables obtained from the coarse solver at time $T_n = \Delta T \cdot n$ before and after the correction from the fine solution, respectively; N_c is the number of the coarse intervals in the entire simulation period; ΔT is the coarse step size. The superscript denotes the iteration number, i.e., superscript "0" represents the initial coarse propagation.

Starting from the first iteration, the fine solver $F_{\delta t}$ takes the coarse solution from the last iteration as the initial value to propagate the solution in each coarse interval:

$$\mathbf{u}_n^k = F_{\delta t}(\mathbf{U}_{n-1}^{k-1}),\ \forall 1 \le n < N_c, \tag{4.2}$$

where $\mathbf{u}_n$ is the vector of state variables obtained from the fine solver at time T_n; δt is the fine step size.

Once the fine solution $\mathbf{u}_n$ is obtained for all $1 \le n < N_c$, the mismatch between the fine solution from the current iteration and the coarse solution from the last iteration $\mathbf{\Delta}_n$, at the time point T_n, can be calculated as:

$$\mathbf{\Delta}_n^k = \mathbf{u}_n^k - \tilde{\mathbf{U}}_n^{k-1},\ \forall 1 \le n < N_c. \tag{4.3}$$

Before moving to the next iteration, the mismatch $\mathbf{\Delta}_n$ is added to the coarse solution from the last iteration as a correction. Note that this correction is not executed simultaneously for all T_n. It is executed sequentially moving along the time T_n:

$$\begin{aligned} \mathbf{U}_n^k &= \tilde{\mathbf{U}}_n^k + \mathbf{\Delta}_n^k, \\ \tilde{\mathbf{U}}_n^k &= C_{\Delta T}(\mathbf{U}_{n-1}^k) \end{aligned} \tag{4.4}$$

Since the coarse propagation is performed for each time point T_n it is critical that the coarse solver $C_{\Delta T}$ is as fast as possible.

The ideal speedup R_{ideal} for Parareal algorithm does not consider the sequential coarse propagation, i.e. it is assumed to be negligible:

$$R_{ideal} = \frac{N_c}{N_{iter}}. \tag{4.5}$$

where N_{iter} is the number of correction iterations.

However, the actual speedup R_{act} is influenced by the coarse propagations:

$$R_{act} = \frac{T_{seq}}{T_{Par}}, \tag{4.6}$$

where T_{seq} is the sequential simulation time, T_{Par} is the total simulation time of the Parareal algorithm which includes the time consumed to propagate the fine solution and the coarse solution for each iteration.

4.1.2 Power system model

The power system model used in this section includes the detailed generator model, the non-reheat steam turbine model, the first-order governor model and the IEEE type 1 exciter model. The models are represented by a system of 15 differential equations:

$$\begin{cases}
T_{sv_i}\dot{P}_{sv_i} = -P_{sv_i} + P_{c_i} - s_i / R_i \\
T_{ch_i}\dot{T}_{m_i} = -T_{m_i} + P_{sv_i} \\
T_{E_i}\dot{E}_{fd_i} = -\left(K_{E_i} + A_{E_i}\exp(B_{E_i}E_{fd_i})\right)E_{fd_i} + V_{R_i} \\
T_{F_i}\dot{V}_{2_i} = -V_{2_i} + E_{fd_i}K_{F_i} / T_{F_i} \\
T_{R_i}\dot{V}_{1_i} = -V_{1_i} + V_{t_i} \\
T_{A_i}\dot{V}_{R_i} = -V_{R_i} + K_{A_i}V_{2_i} - E_{fd_i}K_{A_i}K_{F_i} / T_{F_i} + K_{A_i}\left(V_{ref_i} - V_{1_i}\right) \\
\dot{\delta}_i = \omega_b s_i \\
2H_i\dot{s}_i = T_{m_i} - T_e - D_i s_i \\
\dot{\psi}_{f_i} = -\psi_{f_i}\omega_b R_{f_i} / X_{fl_i} + \psi_{ad_i}\omega_b R_{f_i} / X_{fl_i} + E_{fd_i}\omega_b R_{f_i} / X_{ad_i} \\
\dot{\psi}_{h_i} = -\psi_{h_i}\omega_b R_{h_i} / X_{hl_i} + \psi_{ad_i}\omega_b R_{h_i} / X_{hl_i} \\
\dot{\psi}_{g_i} = -\psi_{g_i}\omega_b R_{g_i} / X_{gl_i} + \psi_{aq_i}\omega_b R_{g_i} / X_{gl_i} \\
\dot{\psi}_{k_i} = -\psi_{k_i}\omega_b R_{k_i} / X_{kl_i} + \psi_{aq_i}\omega_b R_{k_i} / X_{kl_i} \\
T_c\dot{E}''_{dc_i} = -E''_{dc_i} - \left(X''_{qs_i} - X''_{ds_i}\right)i_{q_i} \\
T_{xd_i}\dot{X}''_{ads_i} = -X''_{ads_i} + F_{d_i} \\
T_{xq_i}\dot{X}''_{aqs_i} = -X''_{aqs_i} + F_{q_i}
\end{cases} \tag{4.7}$$

where

$$T_{e_i} = E''_{d_i} i_{d_i} + E''_{q_i} i_{q_i} + \left(X''_{ads_i} - X''_{aqs_i} \right) i_{q_i},$$

$$\psi_{ad_i} = X''_{ads_i} i_{d_i} + E''_{q_i}, \qquad \psi_{aq_i} = X''_{aqs_i} i_{q_i} + E''_{d_i},$$

$$i_{d_i} = \frac{\left(E''_{d_i} - V_t \sin(\theta_{t_i} - \delta_i) \right) R_a - \left(E''_{q_i} - V_t \cos(\theta_{t_i} - \delta_i) \right) X''_{qs_i}}{R_a^2 + X''_{ds_i} X''_{qs_i}},$$

$$i_{q_i} = \frac{\left(E''_{q_i} - V_t \cos(\theta_{t_i} - \delta_i) \right) R_a - \left(E''_{d_i} - V_t \sin(\theta_{t_i} - \delta_i) \right) X''_{ds_i}}{R_a^2 + X''_{ds_i} X''_{qs_i}},$$

$$X''_{ds_i} = X''_{ads_i} + X_{l_i}, \qquad X''_{qs_i} = X''_{aqs_i} + X_{l_i},$$

$$E''_{d_i} = \left(\frac{\psi_{f_i}}{X_{f_i}} + \frac{\psi_{h_i}}{X_{h_i}} \right) X''_{ads_i}, \qquad E''_{q_i} = -\left(\frac{\psi_{g_i}}{X_{g_i}} + \frac{\psi_{k_i}}{X_{k_i}} \right) X''_{aqs_i}.$$

Here, T_c, T_{xd_i}, T_{xq_i} are time constants of dummy coils all in s; s_i is the generator rotor slip; T_{m_i} and T_e are the mechanical torque and electrical torque; V_{2_i} is the rate feedback; θ_{t_i} is the terminal bus voltage angle in rad; ψ_{f_i}, ψ_{h_i}, ψ_{g_i}, ψ_{k_i}, R_{f_i}, R_{h_i}, R_{g_i}, R_{k_i}, X_{fl_i}, X_{hl_i}, X_{gl_i} and X_{kl_i} are respectively field, h-, g-, and k-winding flux linkages, reluctances and leakage reactances; ψ_{ad_i}, ψ_{aq_i}, X''_{ds_i}, X''_{qs_i}, X''_{ads_i}, X''_{aqs_i}, F_{d_i} and F_{q_i} are respectively d- and q-axis mutual flux linkages, saturated subtransient reactances, saturated mutual subtransient reactances and saturation components; E''_{dc_i} is the dummy

coil voltage; X_{ad_i}, R_a and X_{l_i} are the mutual synchronous reactance, armature resistance and leakage reactance.

The above-mentioned algebraic equations are substituted into the system of differential equations in (4.7) so that all differential equations are functions of state variables and terminal bus voltage magnitudes and angles. Thus, the terminal bus voltage phasors are the inputs in the system and are used to connect the algebraic solver that performs power system network calculations with the differential solver that calculates the states of the system.

The resulting model can be described with the following nonlinear system:

$$\begin{cases} \dot{\mathbf{x}} = \mathbf{f}\left(\mathbf{x}, \mathbf{u}\right) \\ \mathbf{y} = \mathbf{x} \end{cases} \tag{4.8}$$

where

$$\mathbf{u} = \left(\boldsymbol{\theta} \quad \mathbf{V}_t\right)^T,$$

$$\mathbf{x} = \left(\mathbf{P}_{sv} \quad \mathbf{T}_m \quad \mathbf{E}_{fd} \quad \mathbf{V}_2 \quad \mathbf{V}_R \quad \boldsymbol{\delta} \quad \boldsymbol{\omega} \quad \boldsymbol{\psi}_f \quad \boldsymbol{\psi}_h \quad \boldsymbol{\psi}_g \quad \boldsymbol{\psi}_k \quad \mathbf{E}''_{dc} \quad \mathbf{X}_{ads} \quad \mathbf{X}_{aqs}\right),$$

$$\mathbf{x} \in \mathrm{R}^n, \qquad \mathbf{u} \in \mathrm{R}^n, \qquad \mathbf{y} \in \mathrm{R}^m, \qquad n = 14N_g, \qquad m = 2N_g.$$

Based on the model in (4.7) the following hybrid system model of the adaptive model reduction without system partitioning is created:

$$\begin{cases} \dot{\mathbf{x}} = \begin{pmatrix} \hat{\mathbf{f}}\left(\mathbf{x}, \mathbf{u}\right) \\ \hat{\mathbf{A}}\Delta\tilde{\mathbf{x}} + \hat{\mathbf{B}}\Delta\mathbf{u} + \hat{\mathbf{x}}^0 \end{pmatrix} \\ \mathbf{y} = \mathbf{x} \end{cases} \tag{4.9}$$

The model in (4.9) is similar to the one in (2.16) with the addition of the control matrix $\hat{\mathbf{B}}$ representing the connection between the generator states and the generator terminal bus voltage magnitudes and angles.

4.1.3 Case study

The adaptive approach is applied to the coarse solver of the master-workers Parareal method and compared with the original coarse solver. The test is performed on the large-scale 327-machine 2383-bus Polish system. A study area is specified in the system. The study area consists of 29 buses and 8 generators. The external area is set to be the rest of the system that has 319 generators. The study area and the external area are connected by three tie-lines as shown in Figure 4.2.

A case study is performed to find the largest disturbance in the system. The critical clearing time for a three-phase short-circuit fault at every bus in the study area has been found and compared. Bus 2274 has the largest CCT of 0.4 seconds (24 cycles) and the three-phase short-circuit at this bus is selected as the largest disturbance. In another case study, all generator angle deviations have been calculated and ranked. Generator 2197 has the largest angle deviation and is used as a reference to compare the adaptive approach with the original system. The results of simulations are shown in Figure 4.3 and Figure 4.4. It can be seen from Figure 4.3 and Figure 4.4 that the adaptive approach maintains the same accuracy.

As stated previously, the main contributing factor to the time performance of the Parareal method is the number of coarse correction iterations. Hence, the parameters of the

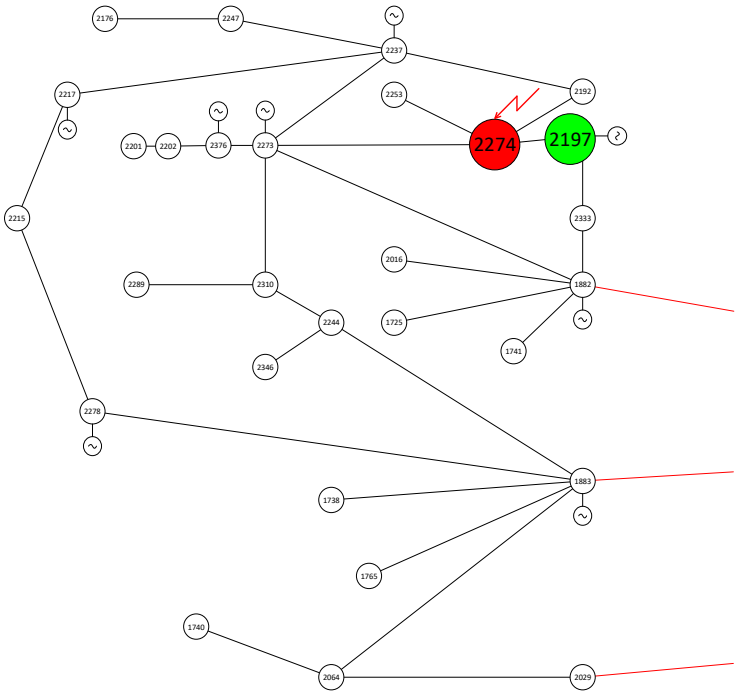

Figure 4.2. Study area of the Polish system.

adaptive approach are selected to maintain the same number of correction iterations. The admittance threshold is set to 0.1 p.u. which corresponds to linearization of nonlinear functions of 281 out of 327 generators. The angle deviation threshold $\Delta\delta_{\max}$ is set to five times the coarse correction threshold: $0.01\times 5 = 0.05$ rad. Both the original and the adaptive coarse solver have the same number of iterations that are shown in Figure 4.5.

Parareal simulation is performed using MATLAB on 16 cores of a 2.6-Ghz Intel Xeon E5-2650 processor with the following settings: simulation length of 8 seconds; time window length of 0.32 seconds; 25 time windows; coarse step size of 0.02 seconds; 16 coarse intervals per window; fine step size of 0.002 seconds; 10 fine intervals per coarse interval.

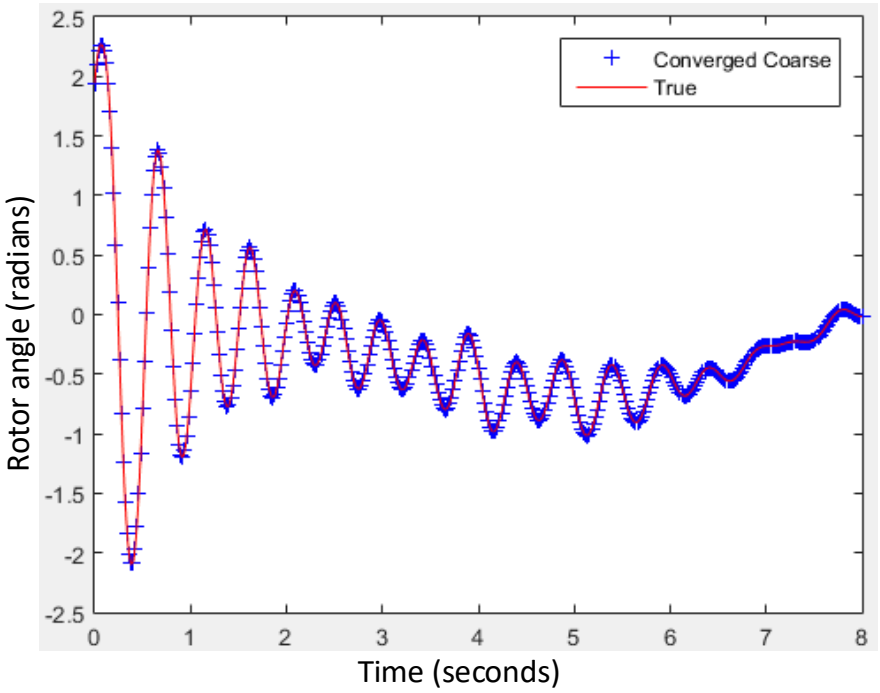

Figure 4.3. Rotor angle of generator 2197 calculated with the original coarse solver.

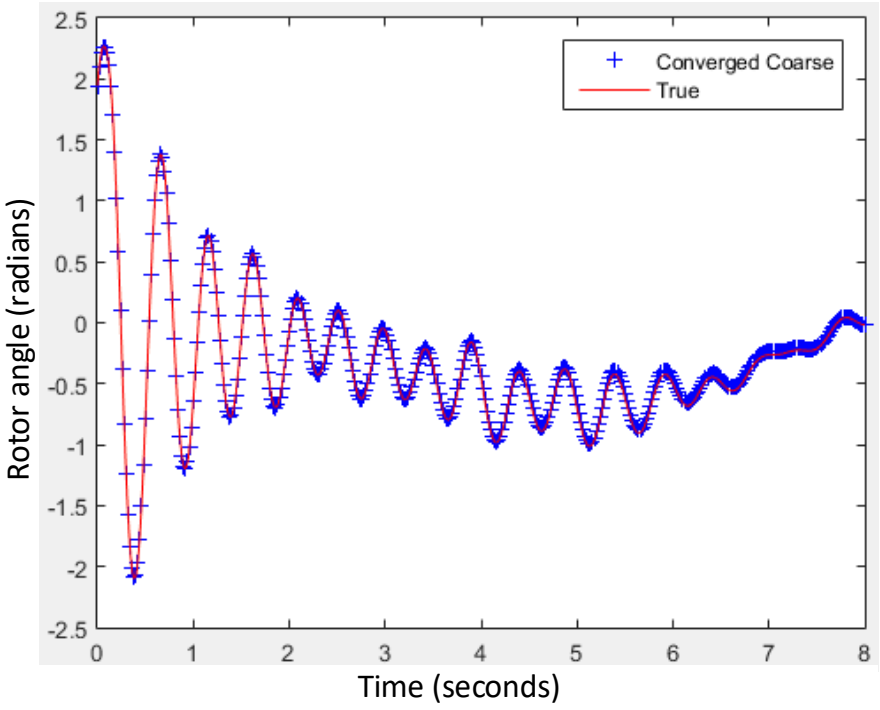

Figure 4.4. Rotor angle of generator 2197 calculated with the adaptive coarse solver.

The number of coarse intervals is set to 16, equal to the number of worker processors used in the simulation. If the number of coarse intervals is less than the number of worker processors, then some of the computing power will not be utilized. Conversely, if the number of coarse intervals is more than the number of worker processors, some of the processors will be overtasked while others undertasked. Thus, as may be expected, the optimal number of coarse intervals for every time window interval is equal to the number of worker processors used in the parallel computing.

The speed performance comparison is given in Table 4.1. The master-workers Parareal method with adaptive model reduction is 47.5% faster than the simulation of the original system and 25% faster than the Parareal simulation with the original coarse solver.

4.2 Distributed Algorithm

4.2.1 Parareal algorithm

At the beginning of the distributed Parareal algorithm processor 0 calculates the initial coarse solution for the first coarse interval:

$$\tilde{\mathbf{U}}_1^0 = C_{\Delta T}(\mathbf{U}_0^0), \tag{4.10}$$

Processor 0 then sends the coarse solution to processor 1 and starts the fine propagation:

$$\mathbf{u}_1^1 = F_{\delta t}(\mathbf{U}_0^0), \tag{4.11}$$

As the fine solution for the first interval is identical to the sequentially propagated solution and no correction is required, the coarse solution for the first interval is equal to the fine

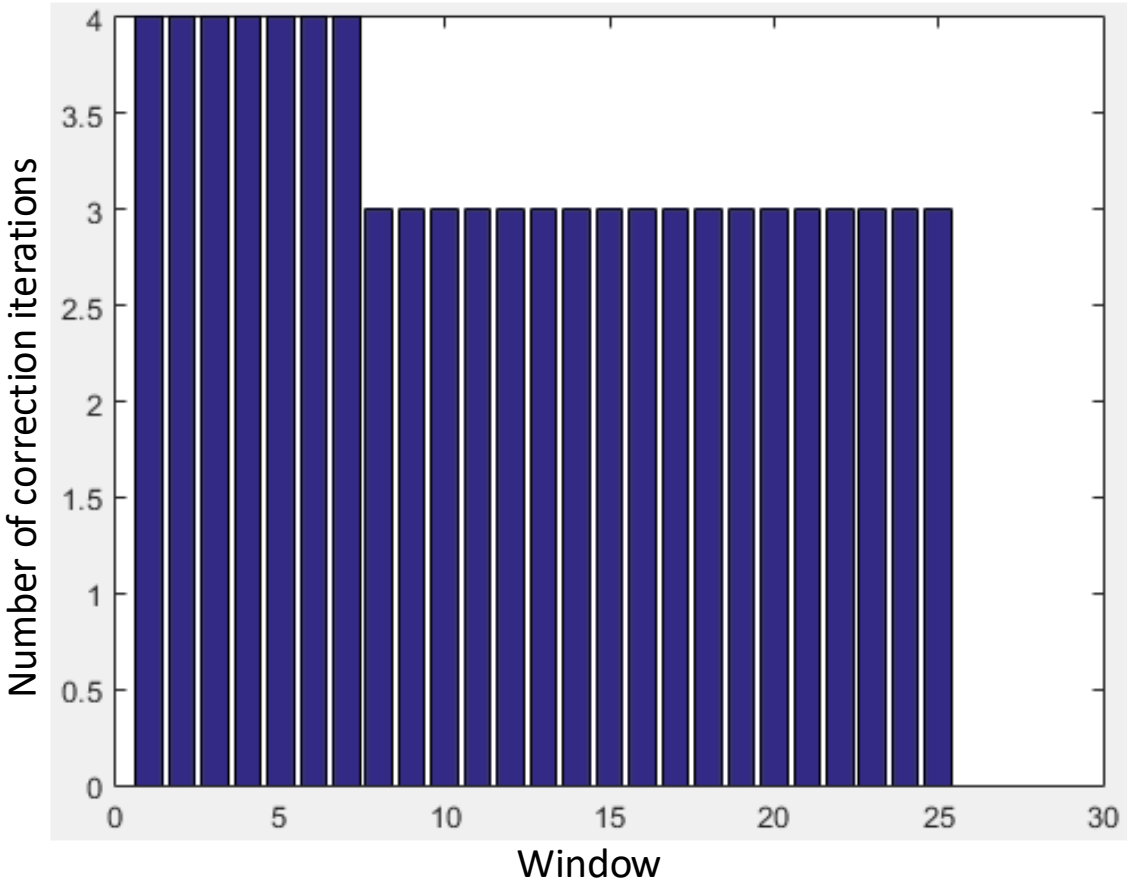

Figure 4.5. Number of correction iterations per window of Parareal simulation.

Table 4.1. Comparison of Master-Workers Parareal Simulation Time

System	Simulation Time (seconds)
Original simulation	40
Parareal simulation with original coarse solver	28
Parareal simulation with adaptive coarse solver	21

solution: $\mathbf{U}_1^1 = \mathbf{u}_1^1$. The solution is sent to processor 1. The coarse propagation continues as processor *id* receives the coarse solution from processor *id-1*, calculates the coarse solution for the next interval:

$$\tilde{\mathbf{U}}_{id+1}^0 = C_{\Delta T}(\tilde{\mathbf{U}}_{id}^0), \tag{4.12}$$

and sends it to processor *id+1*.

After the last processor finishes calculations and the initial coarse propagation is complete, the main part of the distributed algorithm starts. Processor *id* receives the coarse solution form processor *id-1* obtained during the previous iteration, starts the fine propagation:

$$\mathbf{u}_{id+1}^k = F_{\delta t}(\mathbf{U}_{id}^{k-1}). \tag{4.13}$$

By this time processor *id-1* finishes the current iteration, and processor *id* receives the new coarse solution from processor *id-1* and propagates the coarse solution:

$$\tilde{\mathbf{U}}_{id+1}^k = C_{\Delta T}(\mathbf{U}_{id}^k), \tag{4.14}$$

The new coarse solution is corrected based on the fine solution from the current iteration and the coarse solution from the previous iteration:

$$\mathbf{U}_{id+1}^k = \tilde{\mathbf{U}}_{id+1}^k + \mathbf{u}_{id+1}^k + \tilde{\mathbf{U}}_{id+1}^{k-1}, \tag{4.15}$$

At any point if the coarse solution at interval *id* converges, the corresponding processor terminates operations and the calculations continue with the processors corresponding to the later coarse time intervals (*id+1* to N_c).

4.2.2 Non-iterative ZIP load modelling

The power system model used in this section is similar to (4.7) except the additional ZIP loads added to the model compared to the constant impedance loads used in the model from section 4.1.

In the ZIP load model, the active power and reactive power are represented by 3 components: constant impedance (Z), constant current (I), and constant power (P):

$$P_L = a_1 P_{L_o} + a_2 \left(\frac{P_{L_o}}{V_{L_o}} \right) V_L + a_3 \left(\frac{P_{L_o}}{V_{L_o}^2} \right) V_L^2, \tag{4.16}$$

$$Q_L = b_1 P_{L_o} + b_2 \left(\frac{Q_{L_o}}{V_{L_o}} \right) V_L + b_3 \left(\frac{Q_{L_o}}{V_{L_o}^2} \right) V_L^2, \tag{4.17}$$

where V_{L_o}, P_{L_o}, Q_{L_o} are respectively the load bus voltage magnitude, active power, and reactive power at operating condition (equilibrium point); $a_1 + a_2 + a_3 = 1$, a_1, a_2, a_3 are respectively the fractions of constant power, constant current and constant impedance component of the active power; $b_1 + b_2 + b_3 = 1$, b_1, b_2, b_3 are respectively the fractions of constant power, constant current and constant impedance component of the reactive power; V_L is the load bus voltage magnitude.

Active and reactive power are components of the complex power of the load:

$$\bar{S}_L = P_L + jQ_L. \tag{4.18}$$

The current consumed by the load can be calculated as:

$$\bar{I}_L = \left(\frac{\bar{S}_L}{\bar{V}_L} \right)^* . \tag{4.19}$$

where $\bar{V}_L$ is the load bus voltage phasor.

For the case of constant impedance load model when $a_1 = a_2 = b_1 = b_2 = 0$ and $a_3 = b_3 = 1,$ the load can be represented by the load admittance:

$$\bar{Y}_L = \frac{P_{L_o} - jQ_{L_o}}{V_{L_o}^2}. \tag{4.20}$$

Load admittance $\bar{Y}_L$ depends only on the initial conditions and can be absorbed into the network admittance matrix. In general, the load can be represented by a Norton equivalent as shown in Figure 4.6.

Load current injection can then be calculated as:

$$\bar{I}_l = \bar{V}_L \bar{Y}_L - \bar{I}_L. \tag{4.21}$$

If both the active power and reactive power load components are modeled as constant impedance loads, the load current injections $\bar{I}_l$ is equal to zero. For cases of constant power and constant current loads, the value $\bar{I}_l$ is zero only at the operating point. If the system is disturbed and moves away from the initial operating point, $\bar{I}_l$ changes from zero to a new value. The new value is the function of the load bus voltage. In turn, however, the load bus voltage is a function of the current injection. Thus, $\bar{I}_l$ has to be calculated iteratively: 1) calculate the load current injection, 2) solve the system of linear equations $\mathbf{Y} \cdot \mathbf{V} = \mathbf{I}$ (where $\mathbf{Y} \in R^{n \times n}$ is the complex network admittance matrix, **V** is the complex vector of bus voltages, **I** is the complex vector of bus current injections, *n* is the number of

buses) to get a new value of the load bus voltage, then 3) calculate the load current injection again and continue until convergence is achieved.

Iterative solution is time consuming because it takes substantial time to solve the system of linear equations $\mathbf{Y} \cdot \mathbf{V} = \mathbf{I}$ for a large system. To avoid iterative solution, the bus current injection can be calculated by creating 'dummy' state variables [48] for the active and reactive components of the bus current injection:

$$\begin{cases} T_L \dot{I}_{d_r} = -I_{d_r} + \mathrm{Re}(I_l) \\ T_L \dot{I}_{d_i} = -I_{d_i} + \mathrm{Im}(I_l) \end{cases} \tag{4.22}$$

The bus current injection can be obtained by combining active and reactive components in a complex form:

$$\bar{I}_d = I_{d_r} + jI_{d_i}. \tag{4.23}$$

Over time, $\bar{I}_d$ converges to the correct value of $\bar{I}_l$.

4.2.3 Case study

The adaptive model reduction is used in the coarse solver of the distributed Parareal in time method. It is tested on the large-scale 5617-machine 70285-bus Eastern Interconnection (EI) system. A study area is defined to be the Entergy Texas area of the EI system, which consists of 421 buses and 18 generators. The external area is the rest of the system which has 5599 generators. The study area and the external area are connected by six tie-lines. The study area is shown in Fig. 3. Green circles represent generation buses and red circles represent buses on the boundary between the study and the external area.

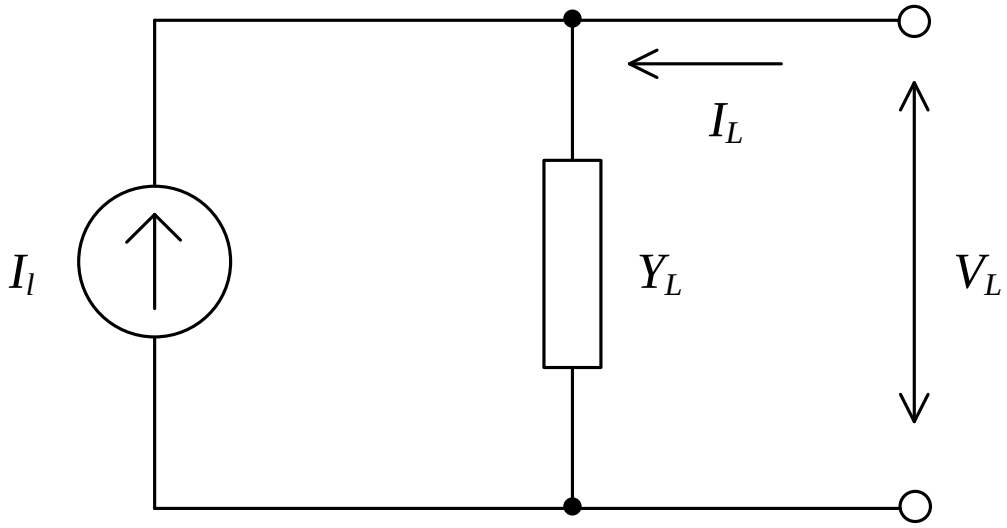

Figure 4.6. Load Norton equivalent.

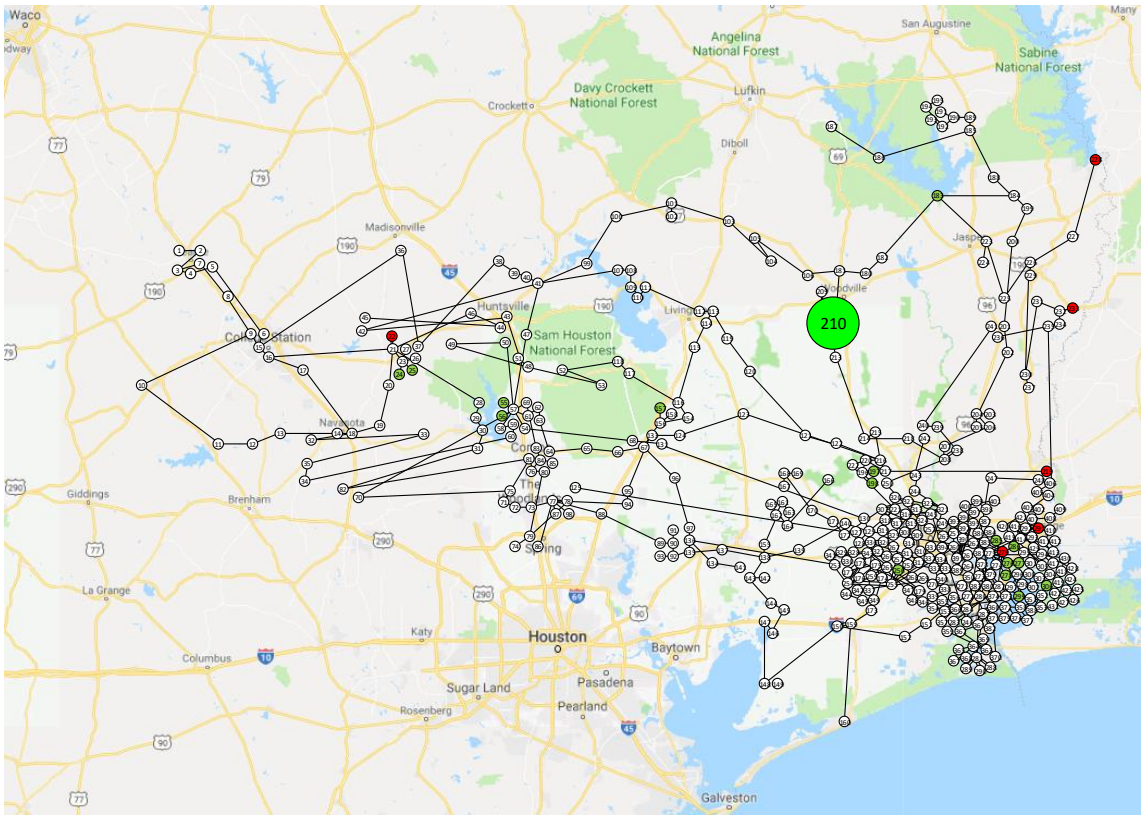

Figure 4.7. Entergy Texas study area.

A typical 4-cycle fault is created on bus 105 inside the study area. Generator 210 is electrically the closest generator to the fault location and is used to demonstrate the Parareal algorithm with the adaptive coarse solver. The results of simulations are shown in Figure 4.8. The adaptive coarse solution successfully converges to the trajectory of the original system simulation.

One of the main contributing factors to the time performance of the Parareal method is the number of coarse correction iterations. The parameters of the adaptive approach are selected in such a way as to maintain the same number of correction iterations. The admittance threshold is set to 0.01 p.u. The angle deviation threshold $\Delta\delta_{max}$ is set to five times the coarse correction threshold: $0.01 \times 5 = 0.05$ rad. Both the original and the adaptive coarse solver have the same number of iterations that is equal to 8.

Parareal simulation is performed using Python in high-performance computing environment with 512 MPI (message passing interface) processors and the following settings: simulation length of 10.24 seconds; coarse step size of 0.02 seconds; fine step size of 0.005 seconds; 4 fine intervals per coarse interval.

The speed performance comparison is given in Table 4.2. The distributed Parareal method with adaptive coarse solver is 98.3% faster than the simulation of the original system producing the speedup of 59 times and 43.7% faster than the Parareal simulation with the original coarse solver.

4.3 Conclusions

In this chapter master-workers and distributed Parareal algorithms with the adaptive approach has been successfully tested on the large-scale Polish and Eastern Interconnection

systems. It has been demonstrated that application of the adaptive model reduction can increase the speed of the coarse solver and reduce the total simulation time of Parareal method. It maintains the same number of correction iterations while performing each iteration faster. Thus, the adaptive approach can provide promising increase in simulation speed for power system transient stability studies.

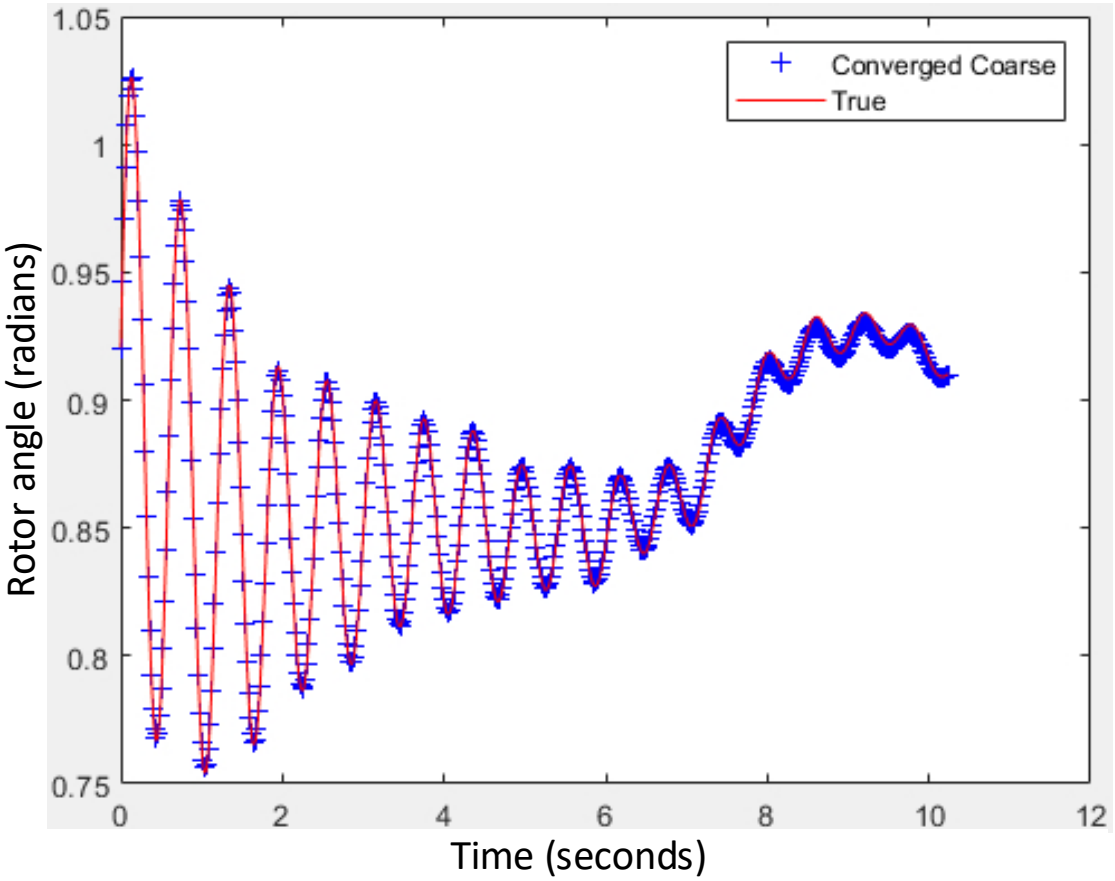

Figure 4.8. Rotor angle of generator 210 following the fault.

Table 4.2. Comparison of Distributed Parareal Simulation Time

System	Simulation Time (seconds)
Original simulation	3193.0
Parareal simulation with original coarse solver	96.1
Parareal simulation with adaptive coarse solver	54.1

CHAPTER FIVE

INTEGRATION OF TENSOR DECOMPOSITION TO ADAPTIVE MODEL REDUCTION

This chapter proposes to use tensor decomposition to represent the Taylor series expansion of a power system dynamic model in order to further improve the speed and accuracy of the adaptive model reduction described in chapter 2.

5.1 Power System Model Approximation

In this chapter, each generator of the power system is represented by a two-axis model with a non-reheat steam turbine model, a first-order governor model and an IEEE type 1 exciter model as described in section 2.4. The system:

$$\begin{cases} \dot{\mathbf{x}} = \mathbf{f}(\mathbf{x}) \\ \mathbf{y} = \mathbf{x} \end{cases} \tag{5.1}$$

can be approximated by Taylor series expansion as shown below in the matrix formulation:

$$\begin{cases} \Delta\dot{\mathbf{x}} = \mathbf{A}_1\Delta\mathbf{x} + \mathbf{A}_2(\Delta\mathbf{x}\otimes\Delta\mathbf{x}) + \mathbf{A}_3(\Delta\mathbf{x}\otimes\Delta\mathbf{x}\otimes\Delta\mathbf{x}) + \cdots \\ \mathbf{y} = \Delta\mathbf{x} + \mathbf{x}_0 \end{cases} \tag{5.2}$$

where $\mathbf{A}_i \in R^{n\times n^i}$ is the matrix of partial derivatives of the functions in (5.1) of order *i*; "$\otimes$" denotes Kronecker product.

In system (5.2) the dimensions of matrices $\mathbf{A}_i$ grow exponentially with the order increase, which in turn increases the computational burden and can make the approximated model in (5.2) even slower than the original model in (5.1). To address this, we propose to

represent matrices $\mathbf{A}_i$ as tensors and apply tensor decomposition to decrease the size of the matrices and improve the speed of computation.

5.2 Tensor Representation

A tensor is a multidimensional array that is defined as $\mathcal{A} \in R^{n_1 \times n_2 \times \cdots \times n_k \times \cdots \times n_d}$, where n_k is the size in dimension *k*, *d* is the number of dimensions. A matrix can be converted to a tensor as shown in the example in Figure 5.1.

Matrices $\mathbf{A}_2, \mathbf{A}_3, \ldots$ in (2) can be converted to tensors $\mathcal{A}_2, \mathcal{A}_3, \ldots$, where $\mathcal{A}_2 \in R^{n_1 \times n_2 \times n_3}$, $\mathcal{A}_3 \in R^{n_1 \times n_2 \times n_3 \times n_4}$, $n_1 = n_2 = n_3 = n_4 = n$. Kronecker product in (5.2) can be represented by the tensor dimension multiplication [49]. A *k*-dimension product of a tensor and a matrix is a tensor of which the entries are calculated as follows [50]:

$$(\mathcal{A} \times_k X)_{j_1 j_2 \cdots j_{k-1} i j_{k+1} \cdots j_d} = \sum_{j_k=1}^{n_k} \mathcal{A}_{j_1 j_2 \cdots j_k \cdots j_d} X_{i j_k}, \tag{5.3}$$

where $\mathcal{A} \times_k X \in R^{n_1 \times n_2 \times \cdots \times n_{k-1} \times m \times n_{k+1} \times \cdots \times n_d}$, $X \in R^{m \times n_k}$.

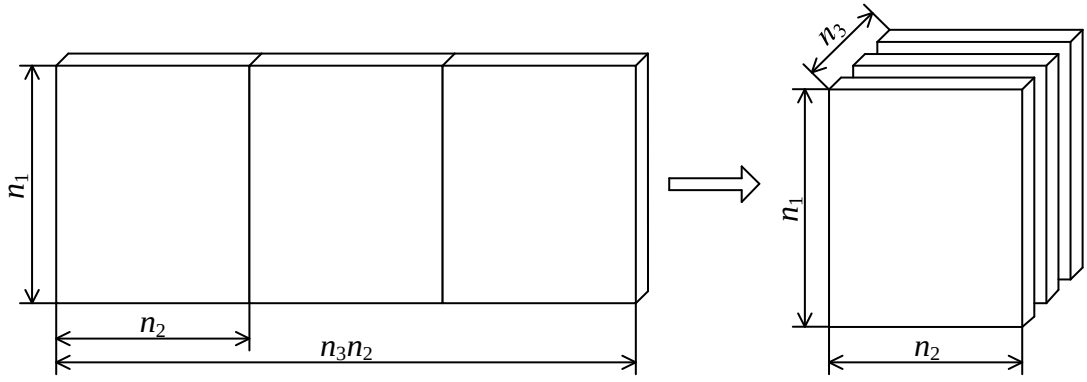

Figure 5.1. Representation of a matrix by a third-order tensor.

The system (5.2) can be rewritten as:

$$\begin{cases} \Delta\dot{\mathbf{x}} = \mathbf{A}_1\Delta\mathbf{x} + \mathcal{A}_2 \times_2 \Delta\mathbf{x}^T \times_3 \Delta\mathbf{x}^T + \mathcal{A}_3 \times_2 \Delta\mathbf{x}^T \times_3 \Delta\mathbf{x}^T \times_4 \Delta\mathbf{x}^T + \cdots \\ \mathbf{y} = \Delta\mathbf{x} + \mathbf{x}_0 \end{cases} \tag{5.4}$$

5.3 Tensor Decomposition

A tensor can be approximated by the sum of a finite number of rank-one tensors using the CANDECOMP/PARAFAC (CP) decomposition [51]. A *d*th-order tensor is rank one if it can be written as the outer product of *d* vectors:

$$\mathcal{A} = a^{(1)} \circ a^{(2)} \circ \cdots \circ a^{(k)} \circ \cdots \circ a^{(d)}, \tag{5.5}$$

where $a^{(k)} \in R^{n_k}$ is the *k*th rank-one component.

CP tensor decomposition can be written as

$$\mathcal{A} \approx \sum_{i=1}^{r} a_i^{(1)} \circ a_i^{(2)} \circ \cdots \circ a_i^{(d)}, \tag{5.6}$$

where *r* is the rank of the decomposed tensor. An example of CP tensor decomposition is illustrated in Figure. 5.2.

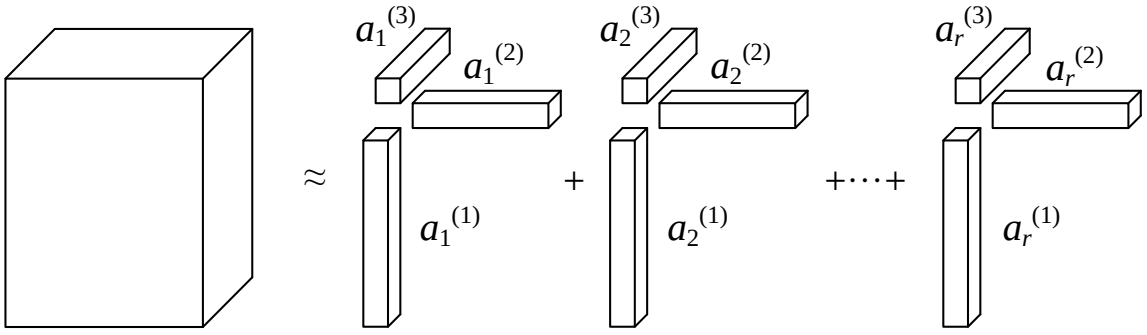

Figure 5.2. CP decomposition of a third-order tensor.

Components in (5.6) which correspond to the same dimension can be grouped into a factor matrix:

$$\mathbf{A}^{(k)} = [a_1^{(k)}, a_2^{(k)}, \ldots, a_r^{(k)}], \tag{5.7}$$

where $\mathbf{A}^{(k)} \in R^{n_k \times r}$.

Factor matrices can be used in one-dimension matricization of a tensor to reconstruct the original matrix [50]:

$$\mathbf{A} \approx \mathbf{A}^{(1)} \left(\mathbf{A}^{(d)} \odot \cdots \odot \mathbf{A}^{(3)} \odot \mathbf{A}^{(2)} \right)^T, \tag{5.8}$$

where "$\odot$" denotes Khatri-Rao product.

Tensors in (5.4) are matricized with the help of (5.8) and the following system is obtained:

$$\begin{cases} \Delta\dot{\mathbf{x}} = \mathbf{A}_1 \Delta\mathbf{x} + \mathbf{A}_2^{(1)} \left(\Delta\mathbf{x}^T \mathbf{A}_2^{(3)} \odot \Delta\mathbf{x}^T \mathbf{A}_2^{(2)} \right)^T \\ \qquad + \mathbf{A}_3^{(1)} \left(\Delta\mathbf{x}^T \mathbf{A}_3^{(4)} \odot \Delta\mathbf{x}^T \mathbf{A}_3^{(3)} \odot \Delta\mathbf{x}^T \mathbf{A}_3^{(2)} \right)^T + \cdots \\ \mathbf{y} = \Delta\mathbf{x} + \mathbf{x}_0 \end{cases} \tag{5.9}$$

5.4 Proposed Hybrid Model Reduction

The proposed model reduction approach is based on partitioning the system into two areas: the study area and the external area. Generators of the study area and generators of the external area electrically close to the boundary between the areas are described by the original nonlinear equations. The model of the rest of generators of the external area is

reduced by approximating it with the Taylor expansion series up to a certain order, which is represented through the tensor decomposition. The resulting hybrid system is described by the following expression:

$$\begin{cases} \Delta\dot{\mathbf{x}} = \begin{pmatrix} \mathbf{A}_1\Delta\mathbf{x} + \mathbf{A}_2^{(1)}\left(\Delta\mathbf{x}^T\mathbf{A}_2^{(3)} \odot \Delta\mathbf{x}^T\mathbf{A}_2^{(2)}\right)^T \\ +\mathbf{A}_3^{(1)}\left(\Delta\mathbf{x}^T\mathbf{A}_3^{(4)} \odot \Delta\mathbf{x}^T\mathbf{A}_3^{(3)} \odot \Delta\mathbf{x}^T\mathbf{A}_3^{(2)}\right)^T + \cdots \\ \hat{\mathbf{f}}(\mathbf{x}) - \mathbf{x}_0 \end{pmatrix} \\ \mathbf{y} = \Delta\mathbf{x} + \mathbf{x}_0 \end{cases} \tag{5.10}$$

5.5 Adaptive Switching Algorithm

As the requirements for the details of the simulated system depend on the severity of a contingency this work proposes the following adaptive algorithm: 1) the original system (5.1) is used during fault condition; 2) the hybrid system (5.10) is used in post-fault condition when system disturbance is large; 3) the Taylor series expansion based system (5.9) is used when system disturbance is small. The adaptive algorithm is shown in Figure 5.3

The size of the disturbance is determined by the maximum rotor angle deviation of all generators of the study area. A generator with large inertia located electrically far away from the boundary between the study area and the external area is selected as the reference generator.

During the simulation the algorithm checks if there is a large change in the system

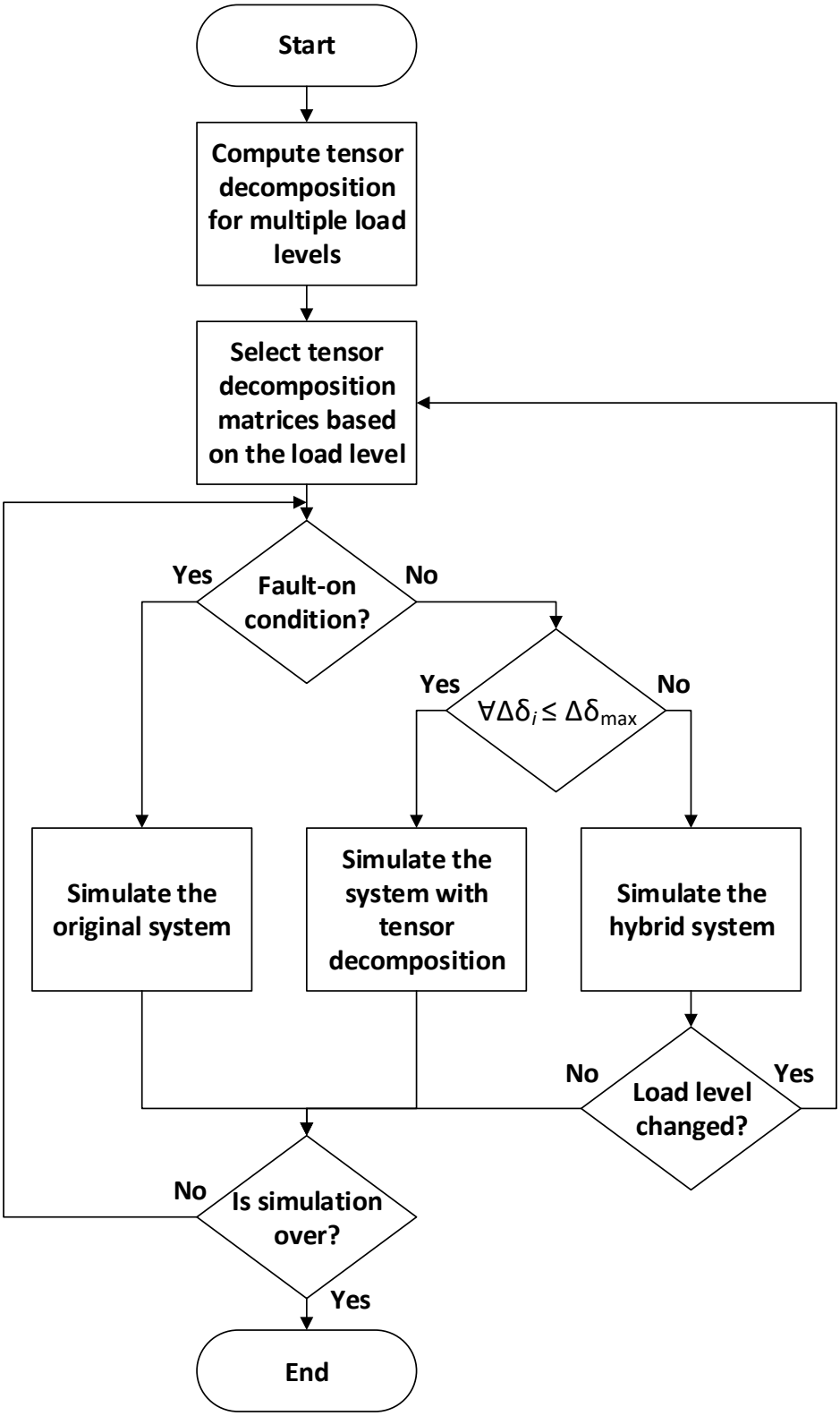

Figure 5.3. Adaptive switching algorithm.

load level. If the load level changes by more than 10% the tensor decomposition matrices are chosen from the set of precalculated ones to correspond to the new load level. This allows the algorithm to maintain the accuracy after a large operating condition change.

5.6 Case Studies

5.6.1 Temporary bus fault tests

The proposed approach is tested on the 140-bus 48-machine NPCC system. The study area is defined as New England part of the system with 36 buses and 9 generators. The external area is defined as the rest of the system with 104 buses and 39 generators.

The threshold for the column norm of the admittance matrix that determines if a generator electrically close to the boundary between the study area and the external area is set to 1 p.u. based on the case study in chapter 2. This corresponds to the approximation of 34 out of 48 generators with the Taylor expansion series. The expansion is performed up to the third order and converted to the tensor format. Tensor decomposition is computed with rank 27 for the second term of the Taylor expansion and with rank 29 for the third one.

The ranks are selected in a case study where the rank is increased from 1 until the increase in rank does not improve the accuracy of the approach in terms of rotor angle by more than 0.1 degrees. Another case study is conducted to set the threshold for the maximum rotor angle deviation that controls the switching between the tensor decomposition only model and the hybrid model. The threshold is increased from 1 degree

until the largest rotor angle error for all generators in the study area is below 5 degrees. The threshold is set to 26 degrees.

The simulations are performed in MATLAB R2015a on a computer with the 4-GHz AMD FX-8350 processor. The simulation length is set to 16 seconds and the integration time step is set to 0.01 seconds.

Based on a case study in chapter 2 the generator with the largest rotor angle error (generator 23) following a fault at the bus (bus 3) with the longest CCT is used to compare the proposed approach with the traditional linear model reduction approach. The results of the comparison are shown in Figure. 5.4.

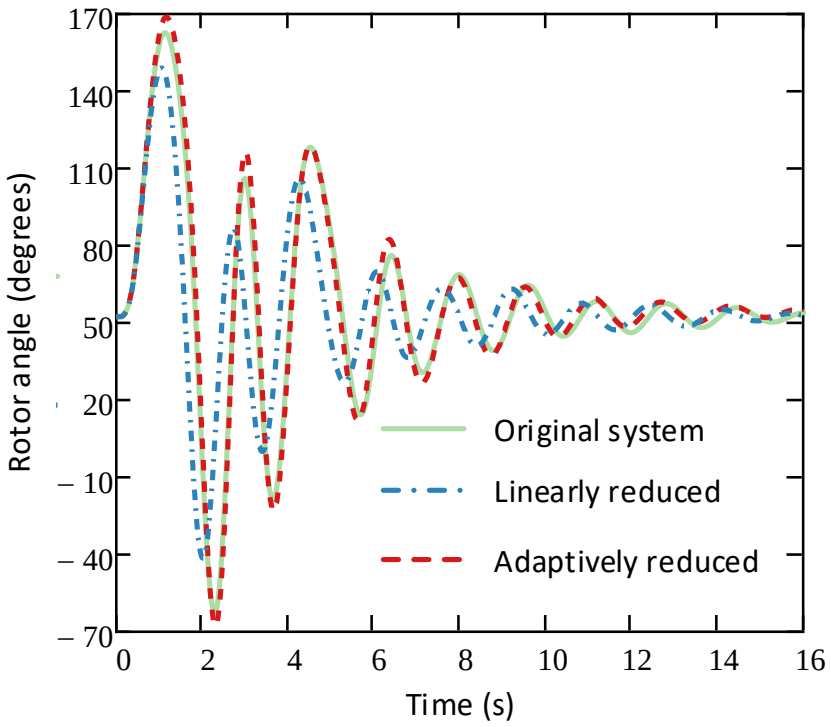

Figure 5.4. Rotor angle of generator 23 following the fault.

The linear model reduction generates a large error while the trajectory simulated with the proposed adaptive model reduction closely follows the trajectory obtained from the original system simulation.

For quantitative comparison the RMS error of the rotor angle is calculated. The RMS error of the linear model reduction is 22.4 degrees while the RMS error of the proposed adaptive model reduction is 4.3 degrees. Thus, the proposed approach reduces the RMS error by 81%.

In addition to accuracy the proposed approach is tested in terms of speed performance. The comparison of the simulation time of the original system, the system simulated with the linear model reduction and the proposed adaptive model reduction are shown in Table 5.1. The proposed approach reduces the simulation time by 76% compare to the original system simulation. The speed performance of the adaptive model reduction is identical to the traditional linear model reduction approach while the accuracy of the simulation is substantially higher.

5.6.2 Test of operating condition change

To test how well the proposed approach performs at different operating conditions, the load level is changed at 5% increments in both heavier and lighter load directions. The fault is set to be at the bus 3 with the duration equal to CCT. The results of the simulations are shown in Table 5.2.

Table 5.2 shows that the accuracy of the proposed approach in terms of the rotor angle remains within 5 degrees at different loading levels. When the load level changes by

Table 5.1. Comparison of Tensor Decomposition Simulation Time

System	Simulation Time (seconds)
Original simulation	3.7
With linear model reduction	0.9
With adaptive model reduction	0.9

Table 5.2. Comparison of Rotor Angle RMS Error at Different Load Levels

Load level (%)	CCT (s)	Load level of tensor decomposition calculation		
		120 %	100 %	80 %
120	0.19	4.1		
115	0.23	3.6		
110	0.27	4.9		
105	0.33		4.9	
100	0.39		4.3	
95	0.44		3.5	
90	0.51			3.5
85	0.59			3.6
80	0.70			4.9

more than 10% the tensor decomposition matrices are changed to the ones obtained from the Taylor series expansion calculated around the equilibrium point with larger or lower load level based on the direction of load change. Thus, the adaptive model reduction is capable of accurate system representation at different operating conditions.

5.6 Conclusions

This chapter has proposed a tensor decomposition based adaptive model reduction approach that further improves speed of the power system simulation while maintaining a better level of accuracy. The approaches is tested during different load levels and is capable of accurate representation of the original system when there is a change in operating condition.

CHAPTER SIX

CONCLUSIONS

6.1 Contributions

This dissertation has proposed a new adaptive nonlinear model reduction approach. The major contributions of this works are in the following aspects:

1. Hybrid model reduction. In the proposed hybrid model reduction all generators inside the study area and the generators inside the external area that contribute to the dynamics of the study area the most are described by the original nonlinear models, the rest of generators inside the external area are represented by the linearized models. The hybrid reduced model serves as a compromise between accuracy and speed of simulation.
2. Column norms of the admittance matrix. The columns norms of the reduced admittance matrix are proposed to be used as a criterion to judge how close electrically each generator inside the external area is to the boundary between the study area and the external area and, hence, to determine the list of generator models to be linearized in the hybrid reduced model.
3. Unpartitioned model reduction. Unlike most of existing model reduction methods that need to partition the whole power network into a study area with detailed models and an external area with reduced models, the new approach can be applied to the whole system without network partitioning.

4. Adaptive switching algorithm. The proposed adaptive model reduction enables adaptive switching among the original detailed model, the linear reduced model and the hybrid reduced model. The original nonlinear model is used during faults when the highest accuracy is required; the fastest linear reduced model is used when the deviation of all system states is within the threshold; the hybrid model, as a compromise between speed and accuracy, is used when deviation of system states becomes larger than the threshold.
5. Generator rotor angle deviation. The largest rotor angle deviation of the generators inside the study area is proposed to be used as a threshold to define the switching instance between the linear reduced model and the hybrid reduced model.
6. Multiple study subareas. The adaptive model reduction is used in the parallelization in space method where the study area is proposed to be divided into multiple subareas that can be simulated in parallel.
7. Adaptive coarse solver. The adaptive model reduction is proposed to be used as a coarse solver in the parallelization in time Parareal method implemented as the master-workers algorithm and as the distributed algorithm.
8. Tensor decomposition. The tensor decomposition is proposed to be integrated into the adaptive model reduction to further improve speed and accuracy of the approach. Taylor series expansion of the system is calculated around multiple equilibria corresponding to different load levels. The terms of Taylor series

expansion are converted to the tensor formant and reduced into smaller matrices with the help of tensor decomposition.

6.2 Future Work

The following are the potential directions of the future work:

1. Adaptive model reduction based on the nonlinear modal decomposition, where the local modes of the generators inside the external area are eliminated and the local modes of the study area and the inter-area modes of oscillations between the generators inside the study area and the external area are preserved.
2. Hybrid Parareal algorithm, where the coarse solution inside a node of a high-performance computing system is propagated and corrected using the master-workers algorithm, and the coarse propagation between nodes is performed using the distributed algorithm.

LIST OF REFERENCES

[1] J. H. Chow, *Power system coherency and model reduction*. Springer, 2013, pp. 1-3.

[2] A. Chang, M. M. Adibi, "Power system dynamic equivalents," *IEEE Trans. Power App. Syst.*, vol. 89, no. 8, pp. 1737–1744, Nov. 1970.

[3] S. T. Y. Lee, F. C. Schweppe, "Distance measures and coherency recognition transient stability equivalents," *IEEE Trans. Power App. Syst.*, vol. 92, no. 5, pp. 1550–1557, Sep. 1973.

[4] B. Avramovic, P. V. Kokotovic, J. R. Winkelman, J. H. Chow, "Area decomposition for electromechanical models of power systems," *Automatica*, vol. 16, no. 6, pp. 637–648, Nov. 1980.

[5] P. V. Kokotovic, B. Avramovic, J. H. Chow, J. R. Winkelman, "Coherency based decomposition and aggregation," *Automatica*, vol. 18, no. 1, pp. 47–56, Jan. 1982.

[6] U. D. Caprio, "Theoretical and practical dynamic equivalents in multimachine power systems: Part 1: Construction of coherency-based theoretical equivalent," *International Journal of Electrical Power and Energy Systems*, vol. 4, no. 4, pp. 224–232, Oct. 1982.

[7] J. Machowski, A. Cichy, F. Gubina, P. Omahen, "External subsystem equivalent model for steady-state and dynamic security assessment," *IEEE Trans. Power Syst.*, vol. 3, no. 4, pp. 1456–1463, Nov. 1988.

[8] S. Geeves, "A modal-coherency technique for deriving dynamic equivalents," *IEEE Trans. Power Syst.*, vol. 3, no. 1, pp. 44–51, Feb. 1988.

[9] J. H. Chow, R. J. Galarza, P. Accari, W. W. Price, "Inertial and slow coherency aggregation algorithms for power system dynamic model reduction," *IEEE Trans. Power Syst.*, vol. 10, no. 2, pp. 680–685, May 1995.

[10] R. J. Galarza, J. H. Chow, W. W. Price, A. W. Hargrave, P. M. Hirsch, "Aggregation of exciter models for constructing power system dynamic equivalents," *IEEE Trans. Power Syst.*, vol. 13, no. 3, pp. 782–788, Aug. 1998.

[11] F. Ma, V. Vittal, "Right-sized power system dynamic equivalents for power system operation," *IEEE Trans. Power Syst.*, vol. 26, no. 4, pp. 1998–2005, Nov. 2011.

[12] B. C. Moore, "Principal component analysis in linear systems: Controllability, observability and model reduction," *IEEE Trans. Autom. Control*, vol. 26, no. 1, pp. 17–32, Feb. 1981.

[13] A. J. Laub, M. T. Heath, C. C. Paige, R. C. Ward, "Computation of system balancing transformations and other applications of simultaneous diagonalization algorithms," *IEEE Trans. Autom. Control*, vol. 32, no. 2, pp. 115–122, Feb. 1987.

[14] M. G. Safonov, R. Y. Chiang, "A Schur method for balanced-truncation model reduction," *IEEE Trans. Autom. Control*, vol. 34, no. 7, pp. 729–733, Jul. 1989.

[15] S. Liu, "Dynamic-data driven real-time identification for electric power systems," Ph.D. dissertation, Univ. of Illinois at Urbana-Champaign, Urbana, IL, 2009.

[16] C. Sturk, L. Vanfretti, Y. Chompoobutrgool, H. Sandberg, "Coherency-independent structured model reduction of power systems*," IEEE Trans. Power Syst.*, vol. 29, no. 5, pp. 2418–2426, Sep. 2014.

[17] L. T. Pillage, R. A. Rohrer, "Asymptotic waveform evaluation for timing analysis," *IEEE Trans. Comput.-Aided Design Integr. Circuits Syst.*, vol. 9, no. 4, pp. 352–366, Apr. 1990.

[18] P. Feldmann, R. Freund, “Efficient linear circuit analysis by Padé approximation via the Lanczos process,” *IEEE Trans. Comput.-Aided Design Integr. Circuits Syst.*, vol. 14, no. 5, pp. 639–649, May 1995.

[19] E. J. Grimme, “Krylov projection methods for model reduction,” Ph.D. dissertation, Univ. of Illinois at Urbana-Champaign, Urbana, IL, 1997.

[20] D. Chaniotis, “Krylov subspace methods in power system studies,” Ph.D. dissertation, Univ. of Illinois at Urbana-Champaign, Urbana, IL, 2001.

[21] J. Hahn, T. F. Edgar, “An improved method for nonlinear model reduction using balancing of empirical Gramians,” *Computers and Chemical Engineering*, vol. 26, no. 10, pp. 1379–1397, Oct. 2002.

[22] J. Qi, J. Wang, H. Liu, A. D. Dimitrovsky, “Nonlinear model reduction in power systems by balancing of empirical controllability and observability covariances,” *IEEE Trans. Power Syst.*, vol. 32, no. 1, pp. 114–126, Jan. 2017.

[23] K. Fujimoto, J. M. A. Scherpen,”Singular value analysis and balanced realizations for nonlinear systems,” in *Model Order Reduction: Theory, Research Aspects and Applications*, Springer, 2008, pp. 251–272.

[24] E. I. Verriest, “Time variant balancing and nonlinear balanced realizations”, in *Model Order Reduction: Theory, Research Aspects and Applications*, Springer, 2008, pp. 213–250.

[25] M. Rathinam, L. R. Petzold, “A new look at proper orthogonal decomposition,” *SIAM Journal on Numerical Analysis*, vol. 41, no. 5, pp. 1893–1925, 2003.

[26] M. Striebel, J. Rommes, “Model order reduction of nonlinear systems in circuit simulation: status and applications,” in *Model Reduction for Circuit Simulation*, Springer, 2011, pp. 289–301.

[27] S. Wang, S. Lu, N. Zhou, G. Lin, M. Elizondo, M. A. Pai, “Dynamic-feature extraction, attribution, and reconstruction (DEAR) method for power system model reduction,” *IEEE Trans. Power Syst.*, vol. 29, no. 5, pp. 2049–2059, Sep. 2014.

[28] M. L. Crow, M. Ilic, “The parallel implementation of the waveform relaxation method for transient stability simulations, “ *IEEE Trans. Power Syst.*, vol. 5, no. 3, pp. 922-932, Aug. 1990.

[29] M. L. Crow, M. Ilic, “The waveform relaxation method for systems of differential/algebraic equations,” *Math. and Comp. modelling*, vol. 19, no. 12, pp. 67-84, Jun. 1994.

[30] G. Gurrala, A. Dimitrovski, P. Sreekanth, S. Simunovic and M. Starke, “Parareal in time for fast power system dynamic simulations,” *IEEE Trans. Power Syst.*, vol. 31, no.3, pp. 1820-1830, May 2016.

[31] N. Duan, A. Dimitrovski, S. Simunovic, K. Sun, “Applying reduced generator models in the coarse solver of Parareal in time parallel power system simulation,” in *Proc IEEE PES Innovative Smart Grid Technologies Europe (ISGT Europe)*, Oct. 2016

[32] N. Duan, A. Dimitrovski, S. Simunovic, K. Sun, “Embedding spatial decomposition in Parareal in time power system simulation,” in *Proc IEEE PES Innovative Smart Grid Technologies North America (ISGT North America) Conference*, Feb. 2018.

[33] N. Duan, K. Sun, “Power system simulation using the multistage Adomian decomposition method,” *IEEE Trans. Power Syst.*, vol. 32, no. 1, pp. 430–441, Jan. 2017.

[34] N. Duan, K. Sun, “Application of the Adomian decomposition method for semi-analytic solutions of power system differential algebraic equations,” in *Proc IEEE PowerTech*, Sep. 2015.

[35] F. van Belzen, S. Weiland, L. Özkan “Model reduction of multi-variable distributed systems through empirical projection spaces,” in *Proc. IEEE Conference on Decision and Control*, Dec. 2009, pp. 5351-5356.

[36] F. van Belzen, “Approximation of multi-variable signals and systems : a tensor decomposition approach,” Ph.D. dissertation, Eindhoven Univ. of Technology, Eindhoven, 2011.

[37] A. Chaudhury, I. Oseledets, R. Ramachandran, “A computationally efficient technique for the solution of multi-dimensional PBMs of granulation via tensor decomposition,” *Comput. Chem. Eng*, vol. 61, pp. 234–244, Feb. 2014.

[38] H. Liu, L. Daniel, N. Wong, “Model reduction and simulation of nonlinear circuits via tensor decomposition,” *IEEE Trans. Comput.-Aided Design Integr. Circuits Syst.*, vol. 34, no. 7, pp. 1059–1069, Jul. 2015.

[39] J. Deng, H. Liu, K. Batselier, Y. Kwok, N. Wong, “STORM: A Nonlinear Model Order Reduction Method via Symmetric Tensor Decomposition,” in *Proc. Asia South Pac. Design Autom. Conf.*, Jan. 2016, pp. 557–562.

[40] P. W. Sauer, M. A. Pai, *Power System Dynamics and Stability*. Englewood Cliffs, NJ: Prentice Hall, 1998, pp. 183-188.

[41] A. A. Desrochers, R. Y. Al-Jaar, "A method for high order linear system reduction and nonlinear system simplification," *Automatica*, vol. 21, no. 1, pp. 93–100, Jan. 1985.

[42] X. Ma, J. A. De Abreu-Garcia, "On the computation of reduced order models of nonlinear systems using balancing technique," in *Proc. Decision and Control,* 1988, pp. 1165–1166.

[43] A. Verhoeven, J. ter Maten, M. Striebel, R. Mattheij, "Model order reduction for nonlinear IC models," in *System Modeling and Optimization*, Springer, 2007, pp. 476–491.

[44] M. Striebel, J. Rommes, "Model order reduction of nonlinear systems: status, open issues, and applications," Chemnitz University of Technology, Chemnitz, Germany, CSC/08-07, Nov. 2008.

[45] B. Wang, K. Sun, "Formulation and characterization of power system electromechanical oscillations," *IEEE Trans. Power Syst.*, vol. 31, no. 6, pp. 5082–5093, Nov. 2016.

[46] E. Aubanel, "Scheduling of tasks in the parareal algorithm," *Pararell Computing*, vol. 37, no. 3, pp. 172–183, Mar. 2011.

[47] H. El-Rewini, M. Abd-El-Barr, *Advanced computer architecture and parallel processing*. Hoboken, NJ: Wiley, 2005, pp. 77-123.

[48] K. N. Shubhanga, *Power system analysis: A dynamic perspective*. Uttar Pradesh, India: Peasson India Eduction Services, 2018, pp. 653-654.

[49] T. G. Kolda, (2006, Apr.). Multilinear operators for higher-order decompositions. Sandia National Laboratories, Livermore, CA.

[50] L. de Lathauwer, B, de Moor, J. Vandewalle, “A multilinear singular value decomposition,” *SIAM Review*, vol. 21, no. 4, pp. 1253–1278, Aug. 2000.

[51] T. Kolda, B. Bader, “Tensor decomposition and applications,” *SIAM Review*, vol. 51, no. 3, pp. 455–500, Aug. 2009.

APPENDIX

Journal Papers

[J1] **D. Osipov**, K. Sun, "Tensor decomposition based adaptive model Reduction for power system simulation," *IEEE Trans. Power Syst.*, in review.

[J2] J. D. Boles, Y. Ma, J. Wang, **D. Osipov**, L. M. Tolbert, F. Wang, "Converter-based emulation of battery energy storage systems (BESS) for grid applications," *IEEE Trans. Ind. Appl.*, in review.

[J3] **D. Osipov**, K. Sun, "Adaptive nonlinear model reduction for fast power system simulation," *IEEE Trans. Power Syst.*, vol. 33, no. 6, pp. 6746–6754, Nov. 2018.

Conference Papers

[C1] **D. Osipov**, N. Duan, S. Allu, S. Simunovic, A. Dimitrovski, K. Sun, "Distributed Parareal in time with adaptive coarse solver for large scale power system simulations," *IEEE PES General Meeting*, Atlanta, 2019, in review.

[C2] **D. Osipov**, N. Duan, A. Dimitrovski, S. Allu, S. Simunovic, K. Sun, "Adaptive model reduction for Parareal in time method for transient stability simulations," *IEEE PES General Meeting*, Portland, 2018.

[C3] **D. Osipov**, F. Hu, K. Sun, "Voltage stability margin estimation for a load area using a three-bus equivalent," *IEEE PES General Meeting*, Boston, 2016.

[C4] M. Nakmali, **D. Osipov**, K. Sun, "A new hybrid approach to Thevenin equivalent estimation for voltage stability monitoring," *IEEE PES General Meeting*, Denver, 2015.

VITA

Denis Osipov received his B. S. and M. S. degrees in electrical engineering from Donetsk National Technical University, Donetsk, Ukraine in 2004 and 2005 respectively. In 2014 he started his Ph.D. program in electrical engineering at the Department of Electrical Engineering and Computer Science, University of Tennessee, Knoxville, TN, USA. His research interests include power system voltage stability, power system model reduction and high-performance computing.